

Characteristics and effectiveness of Atmospheric Motion Vector product (AMV) in Japanese long-term Reanalysis project (JRA-25)

Ryo OYAMA*

Abstract

The Japan 25-year reanalysis (JRA-25) is a project to produce a global and consistent data set of global weather analyses for the years 1979 to 2004. JRA-25 is conducted through collaboration between the Japan Meteorological Agency (JMA) and the Central Research Institute of the Electric Power Industry (CRIEPI). The analysis data would enable users to acquire accurate global climate changes, to enhance seasonal prediction models and to investigate the past global climate and meteorological events via three-dimensional and spatially uniform approach.

This paper reports the quality and characteristics of Atmospheric Motion Vector (AMV) data and AMV impacts on the analysis fields of wind and other physical values in JRA-25. It is recognized that Meteorological Satellite Center (MSC) AMVs, the Meteorology Satellite (METEOSAT) AMVs over the entire period and the Geostationary Operational Environmental Satellite (GOES) AMVs before 1995 contain wind speed slow biases in the upper troposphere, particularly in the winter hemisphere, and that the slow biases decrease year by year. These characteristics correspond to those seen in the ECMWF 15-year reanalysis project (ERA-15).

To verify the impacts of the AMVs on the reanalysis fields, some observation system experiments (OSE) for July 2003 are performed. Through the assimilation of AMVs over the tropical Indian Ocean, upper tropospheric easterly winds and anticlockwise circulation are modified so that the upper and lower tropospheric horizontal divergence field are changed. Over the tropical eastern Pacific Ocean, upper and lower tropospheric wind fields are modified so that lower tropospheric convergence around the Intertropical Convergence Zone (ITCZ) is strengthened. The modifications of the lower tropospheric convergence over both regions mainly induce changes in the precipitation fields. Evaluation of the precipitation fields by the Climate Prediction Center (CPC) Merged Analysis Precipitation (CMAP) data shows that the impact on precipitation fields is neutral over the tropical Indian Ocean, and contains a slightly positive bias around the ITCZ over the tropical eastern Pacific Ocean, respectively.

*System Engineering Division, Meteorological Satellite Center
Received September 29, 2006. Revised February 17, 2007.

1. Introduction

The Japan Meteorological Agency (JMA) and the Central Research Institute of the Electric Power Industry (CRIEPI) conducted a reanalysis project called the Japan 25-year reanalysis project (JRA-25). JRA-25 is the first Japanese long-term reanalysis project and the reanalysis period is from 1979 to 2004. The primary purpose of JRA-25 is to provide a consistent and high quality data set of global weather fields.

Prior to JRA-25, the European Centre for Medium-Range Weather forecasts (ECMWF) completed two long-term reanalysis projects, the ECMWF 15 year reanalysis project (ERA-15) and the ECMWF 40 year reanalysis project (ERA-40). Meanwhile, the National Centers for Environmental Prediction (NCEP) and the National Center for Atmospheric Research (NCAR) have conducted the NCEP / NCAR R1 reanalysis since 1948. Furthermore, the NCEP / Department of Energy (DOE) R2 reanalysis has been conducted using a corrected data assimilation system of the R1. The National Aeronautics and Space Administration (NASA) / Data Assimilation Office (DAO) also completed the NASA Goddard Earth Observing System 1 (GEOS1) reanalysis.

As a review of AMVs used in ERA-15 from 1979 to 1993, Källberg and Uppala (1998) investigate their quality and number. In their impact experiment of the AMVs, they indicate that the assimilation of AMVs has a tendency to reduce westerly winds in the analysis wind field on the upper troposphere in the extra-tropics, and slightly weaken the easterly winds on the lower troposphere in the subtropical regions. The AMVs in ERA-15 are spatially sparser than those which are computed by recent derivation methods.

AMV data is used in JRA-25 for purposes of

assimilation. JRA-25 uses two kinds of AMVs computed by recently improved methods as an advance in AMV utilization. On behalf of JRA-25, the Meteorological Satellite Center (MSC) of the JMA reprocessed high-density AMV data from Geostationary Meteorological Satellites (GMS) -3, -4 and -5 for the period from April 1987 to May 2003. This reprocessing is based on the latest MSC operational AMV extraction method (Kumabe, 2004). JRA-25 also uses reprocessed Meteorology Satellite (METEOSAT) AMVs which are reprocessed using a new algorithm and the recalibrated images of METEOSAT-2 and -3 from May 1982 to May 1988. The reprocessed METEOSAT AMVs are also used in ERA-40.

In this paper, following discussion of the historical number and quality of AMVs, their impacts on and importance for JRA-25 are reported. The configurations of JRA-25 and the utilization of observational data are described in section 2. In section 3, the AMVs used in JRA-25 are reviewed. In section 4, the results of the observing system experiment (OSE) to examine the impacts of AMVs in July 2003 are presented. Finally, section 5 follows as a summary.

2. Overview of JRA-25

This section introduces the summary of the assimilation system and observational data used in JRA-25. The details are described in Onogi et al. (2005).

2.1 Forecast and analysis system

JRA-25 produced six-hourly intermittent analysis and forecast fields. The numerical weather prediction (NWP) model used in JRA-25 is the modified JMA global spectrum model (GSM) whose spectral resolution is T106 equivalent to

an approximately 120 km-horizontal grid scale. The number of the vertical levels is 40, while the top level is at 0.4 hPa. The assimilation scheme is a three-dimensional variational method (3D-VAR), which was adopted in the JMA's operational system between September 2001 and February 2005.

2.2 Observational data

In addition to conventional (direct observational) surface data (e.g. meteorological station observations, buoy and ship observations) and upper atmosphere observations (e.g. sonde and aircraft), JRA-25 uses various satellite data, such as AMV data, brightness temperature data from TOVS (TIROS (Television and Infrared Observation Satellite) Operational Vertical Sounder) and ATOVS (Advanced TOVS), precipitable water from SSM/I (Special Sensor Microwave / Imager) and ocean surface winds from scatterometer.

With respect to AMV data, MODIS (Moderate Resolution Imaging Spectroradiometer) polar winds have been computed from successive IR images of the polar orbital satellites TERA and AQUA in recent times. Furthermore, sea surface winds computed from the microwave scatterometer of the Active Microwave Instrument (AMI) / European Remote-sensing Satellite (ERS) -1, 2 and Seawinds / QuikSCAT are available as observational wind data. These data are used in JRA-25. In addition, JRA-25 uses the wind field retrievals surrounding tropical cyclones (TCR) supplied by Fiorino (Fiorino, 2002) and Chinese daily snow depth data.

2.3 Use of observational data

Observational data is qualified in advance of its assimilation. The Quality Control (QC) of JRA-25 consists of specialized QC for each data type by utilizing only observational data, and dynamic

QC. Dynamic QC is a departure check between observation and first guess, and its criteria vary depending on the first guess values. Regarding brightness temperature and sonde temperature data, biases of the data are corrected prior to QC. Spatially dense data such as satellite data is thinned out.

2.4 Land surface analysis and other analysis

Land surface analysis is performed daily by the JMA simple biosphere model. Snow depth analysis is likewise performed daily by the modified JMA operational system which consists of a two-dimensional optimum interpolation (2D-OI) scheme. JRA-25 uses the Centennial in situ Observation-Based Estimates (COBE) analysis (Ishii et al., 2005) as the daily analysis fields of Sea Surface Temperature (SST) and sea ice. Three-dimensional ozone fields are also produced for JRA-25 by JMA in advance and provided to the forecast model.

3. AMV data in JRA-25

In this section, the features and historical quality and number of AMV data sets, which are computed from successive images from the geostationary satellite, are reviewed.

3.1 Characteristics of AMV

AMV data is used over the entire term of JRA-25. AMV data is computed from either geostationary satellite data or polar orbital satellite data (MODIS polar winds). In this investigation, only AMV data from geostationary satellites is reviewed because the data has been computed for a much longer period than MODIS polar wind in the JRA-25 period. They are categorized into three types by data source: IR, VIS and WV winds. IR winds are computed from successive geostationary IR images

Table 1: History of (a) GMS, (b) METEOSAT and (c) GOES AMVs used in JRA-25. SATOB AMVs are an operational report without the QI.

(a)GMS-AMV

Period	Category
January 1979 – February 1987	SATOB AMV
March 1987 – December 1993	Reprocessed high-density AMV (with QI)
January 1994 – December 1996	SATOB AMV
January 1997 – January 2002	Reprocessed high-density AMV (with QI)
February 2002 – September 2002	SATOB AMV
October 2002 – 21 May 2003	Reprocessed high-density AMV (with QI)
22 May 2003 –	SATOB AMV from GOES-9

(b)METEOSAT-AMV

Period	Category
January 1979 – April 1982	SATOB AMV
May 1982 – May 1988	Reprocessed high-density AMV (with QI)
June 1988 – September 1998	SATOB AMV
September 1998 –	Operational high-density AMV (with QI)

(c)GOES-AMV

Period	Category
January 1979 – March 1998	SATOB AMV
Fall of 1996 –	Operational high-density AMV (without QI) (introduce automated correction of the image navigation)
March 1998 –	Operational high-density AMV (without QI) (increase spatial and temporal resolution)

by tracing cirrus for upper tropospheric winds and cumulus for lower tropospheric winds. VIS winds are computed from successive VIS images by tracing lower tropospheric cloud. These two wind data are produced during the operational period of almost all geostationary satellites. WV winds are computed from successive WV images by tracing dark-white patterns of WV images reflecting upper and middle tropospheric water vapor and clouds. WV winds have been obtained from the middle of 1990s, since a WV absorption channel is boarded on the imagers of geostationary satellites. WV wind data is computed from WV images over cloud regions which are covered by upper and / or middle tropospheric clouds, and clear sky regions where there is no cloud or lower tropospheric cloud cover. WV winds over clear sky region whose height is ordinarily assigned at the middle or lower troposphere, is ordinarily of a poorer quality, because a complete method of the calculation

has not yet been established. Hence, JRA-25 does not use this wind data.

There are two indexes to represent the accuracy of AMVs: the Quality Indicator (QI) index and the Recursive Filter Quality Flag (RFF) index. The QI was devised by the European Organization for Exploitation of Meteorological Satellites (EUMETSAT) (Holmlund, 1998), while the RFF was devised by the Cooperative Institute for Meteorological Satellite Studies (CIMSS). Currently, the two indexes are attached to each set of AMV data reported in BUFR (Binary Universal Form for data representation of meteorological data, WMO 1988) format from respective originating centers, and used for the selection of the data to be assimilated in numerical forecasting centers.

3.2 Utilization history of AMVs used in JRA-25

Table 1 shows the history of AMV data used in

Table 2: Criteria for the QI in selecting AMVs for JRA-25 assimilation system

	Height	SH (~20S)	TR (20S~20N)	NH (20N~)	Upper: 400hPa ~ Middle: 700hPa ~ 400hPa Lower: ~700hPa
IR-WIND	Upper	0.75	0.7	0.75	
	Middle	0.6	0.6	0.6	
	Lower	0.6	0.85	0.6	
VIS-WIND	Upper	not used	not used	not used	
	Middle	not used	not used	not used	
	Lower	0.6	0.6	0.6	
WV-WIND	Upper	0.9	0.7	0.9	
	Middle	not used	not used	not used	
	Lower	not used	not used	not used	

JRA-25. MSC reprocessed the past GMS AMVs for JRA-25 using the MSC's newest operational algorithm (Kumabe, 2004). The reprocessed GMS AMVs are computed on 0.5-degree latitude / longitude grids, while the operational AMVs reported in SATOB (Report of Satellite Observation) format are on 1-degree latitude / longitude grids. Another difference with the reprocessed wind from SATOB wind is the attachment of QI.

The reprocessed AMVs between January 1994 and September 2002 were reproduced once again while calculating JRA-25 because it was found that the data during the period of the project was of a low quality. However, because of time restrictions to complete the JRA-25 calculations, JRA-25 could not help using SATOB winds from January 1994 to December 1996 and from February 2002 to September 2002 when the cause of the low quality was inspected by MSC.

With respect to METEOSAT AMVs, JRA-25 uses the reprocessed METEOSAT AMVs, which were reproduced using a new algorithm and the recalibrated images of METEOSAT-2 and -3 (Van de Berg et al., 2002) over the period from May 1982 to May 1988. Since 7 September 1998, operational high-density AMVs reported in BUFR format with the QI are used (Rattenborg, 1998). For the other

periods of the METEOSAT AMVs, SATOB AMVs are used because only that data is available.

With respect to GOES AMVs, JRA-25 uses operationally reported data. The spatial density of the AMVs is high from March 1998 (Daniels et al., 1998). The QI is not attached to the AMVs. Corrections of wind speed bias and height assignment are also applied to GOES-AMV since 1992 (Hayden, 1993). Wind speed corrections increment by 5 percent and height reassignment is applied to winds stronger than 10 m/s using three-dimensional recursive filter objective analysis.

3.3 Quality check of AMVs

Quality control (QC) for AMV data is the same as that for conventional wind data, i.e., dynamic QC and other QCs. In addition, the QI is used to reject low quality AMVs independent of QC, if available. The QI ranges from 0 to 1 and a high QI indicates high quality. Table 2 shows the criteria of the QI used in JRA-25. The criteria are based on the investigation by JMA where some experiments to assimilate METEOSAT AMVs using several different QI criteria are performed (Nakamura, 2004).

Before assimilation, the AMV data is thinned out into 50km-intervals. Regarding the thinning

rate for the reprocessed GMS AMVs, the rate was changed a few times during the period from January 1997 to February 2002 based on the assimilation experiments to investigate thinning rates and QI criteria. The experiments for the investigation were performed while calculating JRA-25 for trials for the more effective assimilation of data.

The observational error values assigned to the AMVs in a data assimilation scheme vary depending on data height and horizontal positioning according to observational accuracy, the computing quality of the AMVs, and spatial representation in the data assimilation system. Observational accuracy is attributed to the spatial resolution and navigation of satellite images. Computing quality includes accuracy and the spatial and time resolution of the data depending on the computing method. Spatial representation is attributed to how the computed data fits into the spatial and time resolution of the assimilation system.

3.4 Use of AMVs during JRA-25 reanalysis period

Figure 1-1 shows the numbers of (a) GMS AMVs, (b) METEOSAT AMVs and (c) GOES AMVs above 400 hPa assimilated in JRA-25. These numbers represent the accumulated numbers of IR and WV winds.

As seen in Figure 1-1(a), a large number of the GMS AMVs are assimilated in the period from 1987 to 1993 because of the use of reprocessed GMS AMVs. The number of data sets from 1994 to 1996 gets smaller because the SATOB AMVs were used. In the period from January 1997 to February 2002, some discontinuities are found due to changes of thinning rates and QI criteria which are explained in section 3.3. It can be recognized that the number of assimilated AMVs from 1997 to 1999 and

from 2000 to February 2002 are somewhat out of proportion to each other, because the thinning rate and QI criteria vary significantly between these two periods. It is also found that the number of AMV from 2000 to February 2002 is about half as large as that from 1987 to 1993 due to the differences in the thinning rate and QI criteria. From February 2002 to September 2002 and after May 2003, the number is small because the operational SATOB AMVs were used in those periods. The number of AMVs from October 2002 to 21 May 2003 is larger because of less thinning and more liberal QI criteria.

As seen in Figure 1-1(b), the number of METEOSAT AMVs is large in the period from 1982 to 1988, since the reprocessed METEOSAT AMVs were used. After 7 September 1998, the number is also large because the operational high-density AMVs were used. The reason for the large variations in the numbers discovered after January 2001 is not clear here.

As seen in Figure 1-1(c), the number of GOES AMVs consisting of GOES-EAST and GOES-WEST become large from 1996, because the spatial high-density production of AMVs began in the fall of 1996 (Nieman et al., 1996). It is considered that the increase of GOES AMVs from 1998 is due to the next implement of spatial high-density production reported by Daniels et al. (1998). However, the trend gaps recognized in 1999, the end of 2001 and 2002 are not clear.

Figures 1-1(a), (b) and (c) all show that the numbers of the upper tropospheric AMVs over the tropics (20S-20N) are larger than those over the northern (20N-60N) and southern (60S-20S) hemispheres, except for the METEOSAT AMVs from January 2001 to March 2002. In addition, seasonal variation can be seen in the sequence of the number of AMVs over the northern and southern

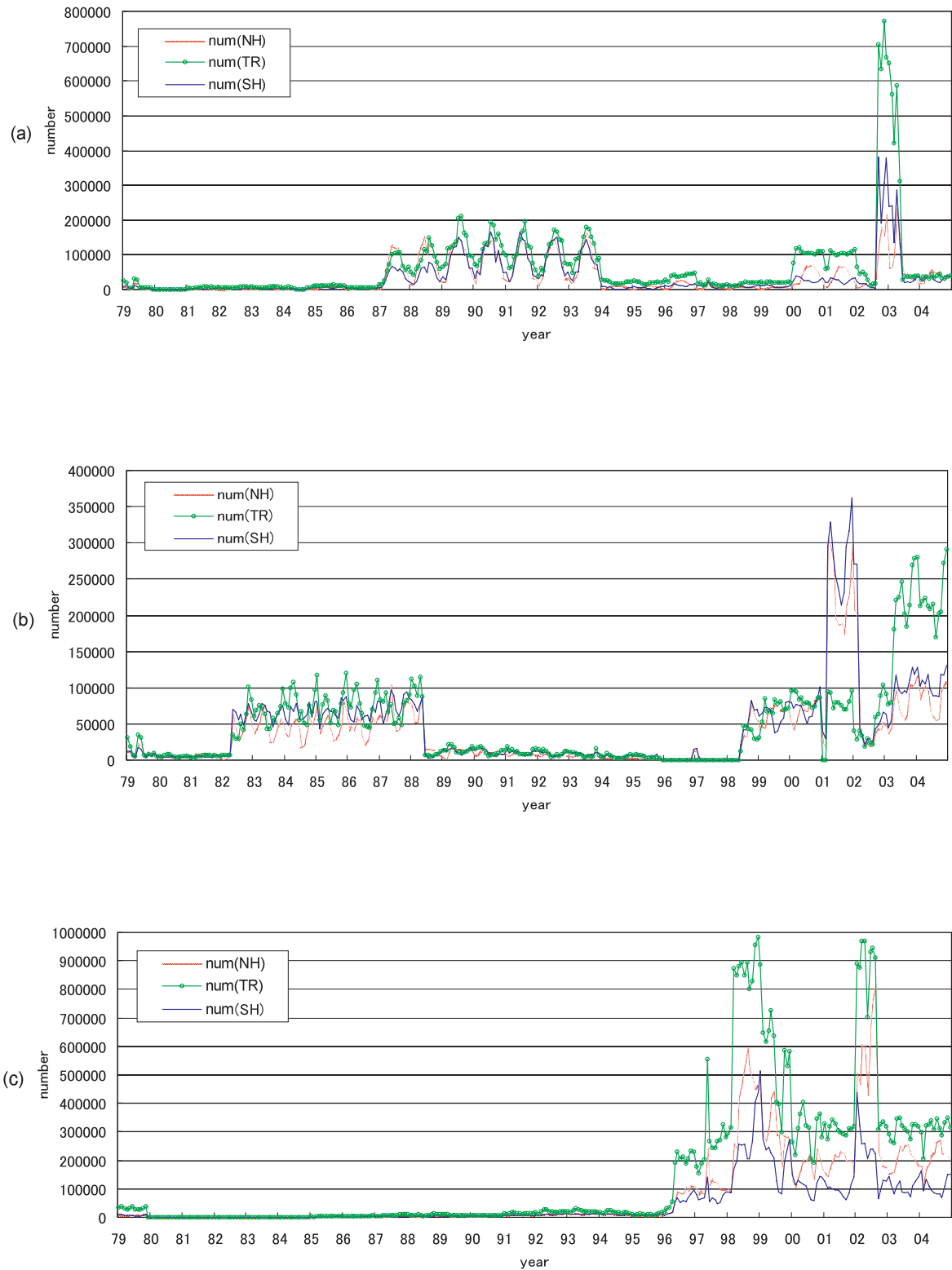


Figure 1-1: Monthly numbers of the (a) GMS AMVs, (b) METEOSAT AMVs and (c) GOES AMVs above 400 hPa. With respect to the GMS AMVs, the data after May 2003 is computed from GOES-9 (positioned at 155E) data. NH, TR, and SH mean Northern hemisphere (between 20N and 60N), Tropics (between 20S and 20N), and Southern hemisphere (between 60S and 20S), respectively.

hemispheres. In general, there is a tendency that numbers in the summer hemisphere are larger than those in the winter hemisphere over the entire period.

3.5 AMV quality during JRA-25 reanalysis period

Figure 1-2 shows the Departure of west-east component (positive for westerly Departure) computed by subtracting the JRA-25 background winds from the AMV winds for the respective satellites. The Departure can be used to evaluate the gap between AMVs and the JRA-25 background winds. The data is above 400 hPa.

The Departures of all satellite AMVs in the upper troposphere tend to be negative values over the northern and southern hemispheres. Over the regions, westerly winds generally blow. Hence, Figure 1-2 may indicate that the AMVs contain a slow bias against the JRA-25 first guess wind field. In the tropics, the bias is very small.

Figure 1-2 (a) shows that the Departures of the GMS AMVs over the northern and southern hemispheres contain seasonal variations. Large Departures can be observed in the winter hemisphere. It can also be observed that the Departures decrease year by year. This trend is clearly seen in the southern hemisphere. The reason is not clear. It is considered that the large Departures before March 1987 are due to the use of the operational GMS AMVs computed by the old derivation process.

Figure 1-2 (b) shows that the seasonal variations in the Departure of the METEOSAT AMVs over the northern and southern hemispheres can be observed except for the non-use period of the AMVs from December 1995 to May 1998. In general, the Departure is small over the tropics. The

interannual variation in the Departure is almost flat between 1979 and 1990, except for the large negative Departures over the northern and southern hemispheres from 1979 to 1982 and from 1988 to 1989 when the SATOB AMV were used. However, the magnitude of Departure over the regions gets rapidly smaller in 1991. After 1999, the magnitude of Departure increases again. The reason for these interannual variations in the Departure is not clear here.

Figure 1-2 (c) shows that the Departures of the GOES AMVs decrease year by year as well. In particular, the changes in the trends in 1987, 1992 and 1996 are distinct. Seasonal variations in Departures are not found after 1996. The reason for the trend gap in 1987 is not clear here. In February 1992, the automated CO2 height assignment method of GOES AMV was introduced (Walter, 1993). In the fall of 1996, a computing method was implemented including the automated correction of image navigation (Nieman et al., 1996). It is possible that these two implementations caused the trend gaps in the Departure in 1992 and 1996, respectively.

According to past investigations of the quality of the GMS AMVs, METEOSAT AMVs, GOES AMVs and INSAT AMVs, used in ERA-15 from 1979 to 1993 (Källberg and Uppala, 1998), the Root Mean Square (RMS) of the difference between the AMV and first guess is gradually improved year by year over the entire period. With respect to the seasonal variations in AMV quality, both situations found in ERA-15 and JRA-25 are very similar; that is, the difference between the AMVs and the first guess is large in the winter hemisphere, though small in the summer hemisphere.

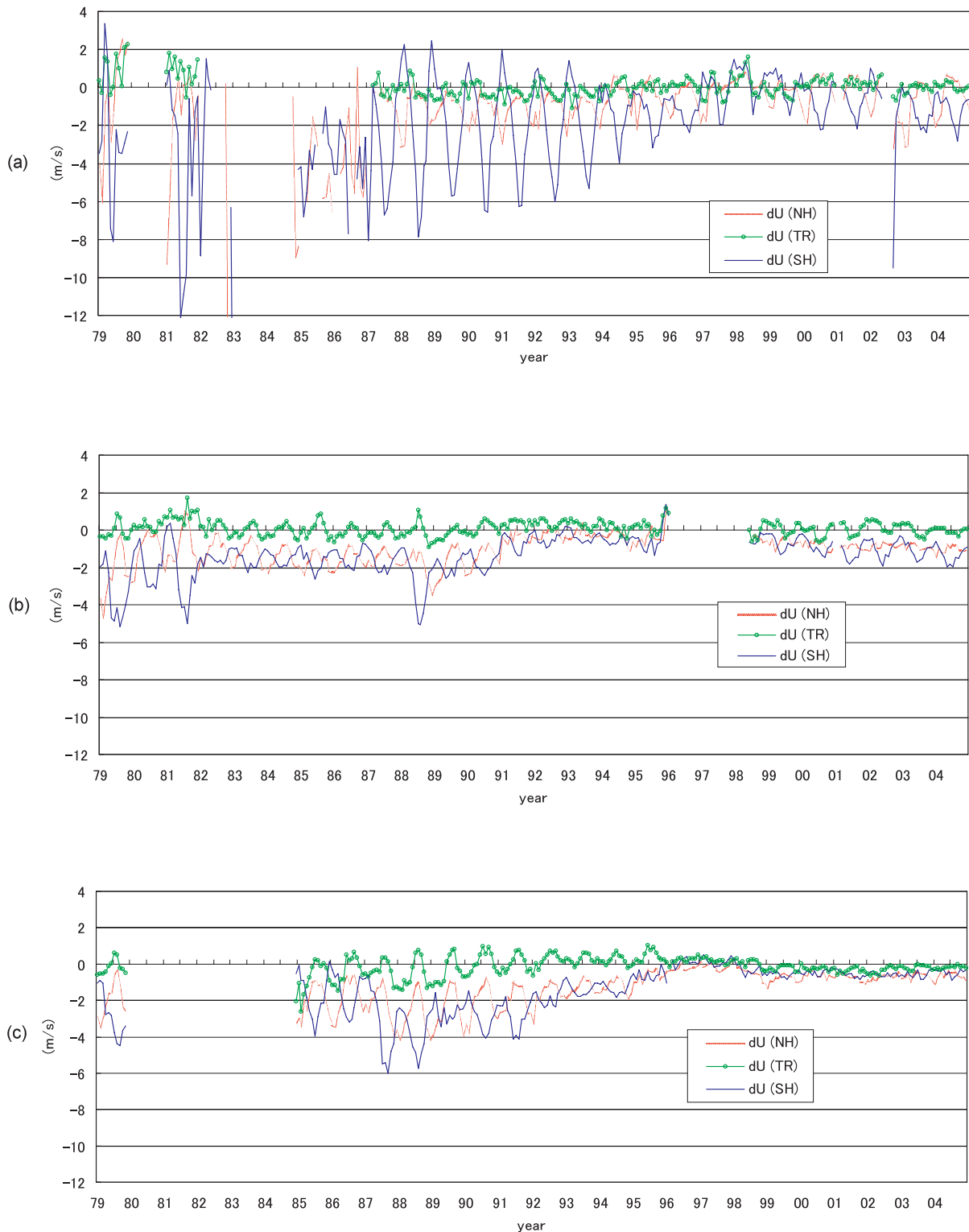


Figure 1-2: One-month averaged west-east component of Departures (data minus JRA-25 first guess) in the (a) GMS AMVs, (b) METEOSAT AMVs and (c) GOES AMVs above 400 hPa. With respect to the GMS AMVs, the data after May 2003 is computed from GOES-9 (positioned at 155E) data. NH, TR and SH mean Northern hemisphere (between 20N and 60N), Tropics (between 20S and 20N) and Southern hemisphere (between 60S and 20S), respectively.

4. Impact study of AMVs for July 2003

4.1 AMV data in July 2003

In this section, AMV data for July 2003, which is used in the observation system experiment (OSE) to investigate the impact of AMVs on JRA-25, is reviewed. In July 2003, there was no particular event such as El Nino or La Nina. Hence, it is considered that the impacts were not affected by any such events; that is, average conditions can be assumed. The AMV data for July 2003 were computed from the observed images of METEOSAT-5 (63 E) and METEOSAT-7 (0 E), GOES-9 (155 E), GOES-10 (135 W) and GOES-12 (75W). In this period, GOES-9 was positioned in the west Pacific region, and its wind data was computed at the MSC of JMA (hereinafter called the MSC-AMV). METEOSAT-5 and 7 AMV data used in JRA-25 were operational high-density data encoded in the BUFR format with the QI. MSC AMV and GOES-10 and -12 AMV data were operationally computed data encoded in the SATOB format without the QI.

Since the computing methods for the METEOSAT-5 and GOES-10 AMVs are the same as those for the METEOSAT-7 and GOES-12 AMVs respectively, here, only the AMV data of GOES-9, METEOSAT-5 and GOES-10 is reviewed.

4.1.1 Height dependency

Figure 2-1 shows the one-month averaged west-east component of the Departure and the monthly numbers of IR winds for (a) GOES-9, (b) METEOSAT-5 and (c) GOES-10 at each height. Hereinafter, the troposphere is divided into three layers: the upper (above 400 hPa), middle (between 700 hPa and 400 hPa) and lower (below 700 hPa) troposphere. The numbers for the middle tropospheric IR winds are smaller than the other

levels for all satellite AMVs. Regarding the IR wind computing method of the MSC AMVs, data was not computed between 501 hPa and 850 hPa, since it is difficult to compute high quality IR winds in the middle troposphere (Ohkawara et. al, 2004).

The magnitude of Departures in the MSC and METEOSAT-5 AMVs in the upper troposphere is relatively larger than those below the layer over the northern (20N-60N) and southern (60S-20S) hemispheres. The Departures in the upper troposphere are negative. Since westerly winds dominate in the upper troposphere over the middle latitudes, Figure 2-1 indicates that the MSC and METEOSAT-5 AMVs in those regions have a slow bias toward the JRA-25 background wind fields. These negative Departures are more clearly observed over the southern hemisphere where it is winter. With respect to the GOES-10 AMVs, the slow biases are smaller than those for the other two satellite AMVs in the upper troposphere. The small biases are mainly caused by the bias adjustment applied to the GOES-10 AMVs.

In the middle troposphere, it can be recognized that the Departures in the METEOSAT-5 and GOES-10 IR winds are negative over the southern hemisphere. With respect to the METEOSAT-5 AMVs, the feature in the middle troposphere is similar to that in the upper troposphere. On the other hand, the negative bias of the Departures in the GOES-10 AMVs in the middle troposphere is more consistent than those in the upper troposphere.

In the lower troposphere, the positive Departures of the IR winds for the three satellites over the tropics and southern hemisphere can be recognized. The magnitudes are approximately 1.0 m/s or smaller. These positive Departures in the three satellites' AMVs are gradually larger as the height

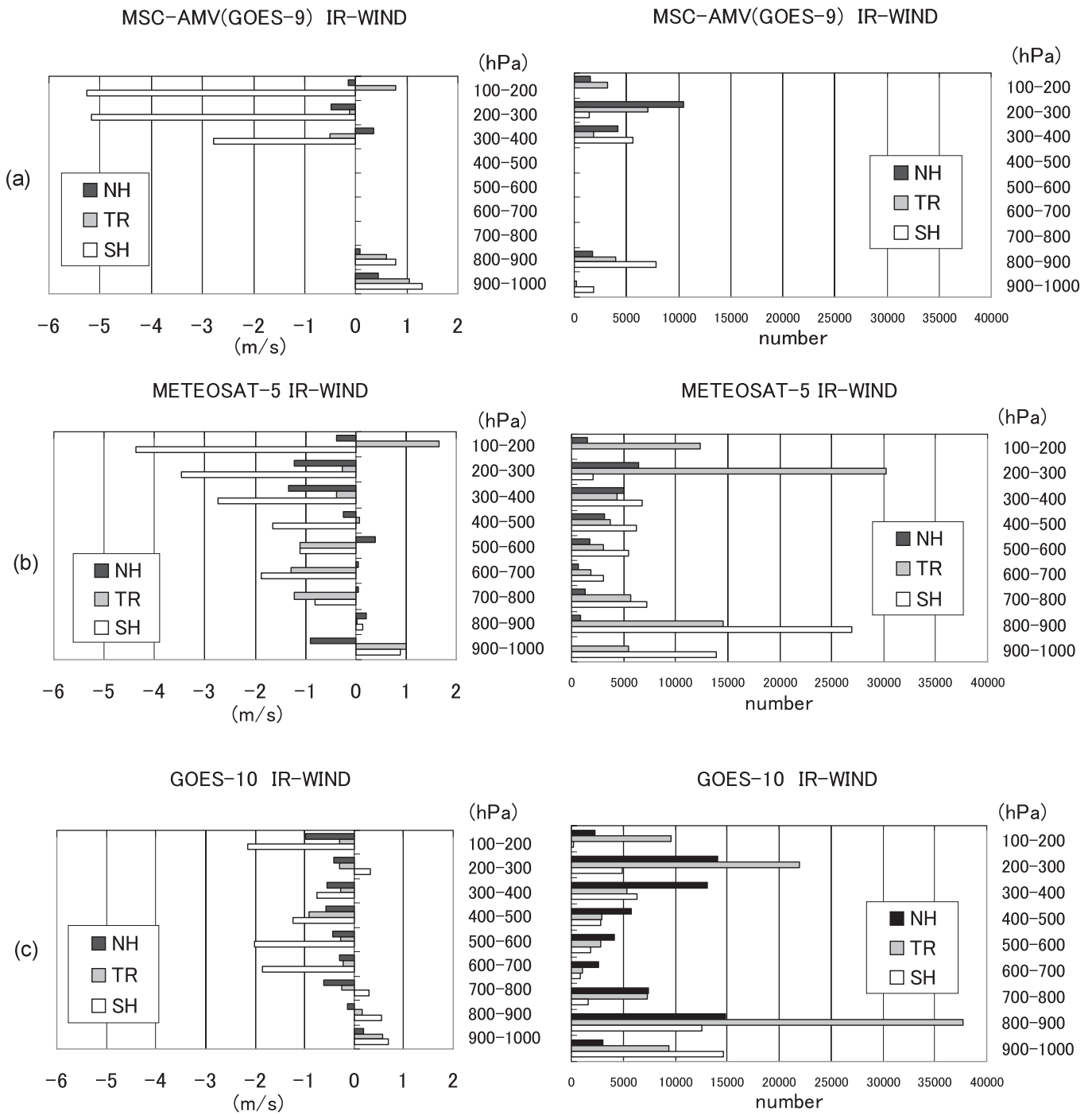


Figure 2-1: One-month averaged west-east component of Departures (data minus JRA-25 first guess) and monthly numbers of each satellite's IR wind at each height. (a) MSC AMVs (GOES-9), (b) METEOSAT-5 AMVs and (c) GOES-10 AMVs. NH, TR and SH mean Northern hemisphere (between 20N and 60N), Tropics (between 20S and 20N) and Southern hemisphere (between 60S and 20S), respectively. The statistical month is July 2003.

is lower. With respect to the northern hemisphere, consistent positive Departures are not apparent for the AMVs of all three satellites.

Figure 2-2 shows the same as Figure 2-1, but for WV winds. The negative Departures in the MSC AMVs and METEOSAT-5 WV winds in the upper troposphere are smaller than those of the IR winds recognized in Figures 2-1 (a) and (b), except for the MSC's WV winds between 100 and 200 hPa over the southern hemisphere, where the number of the data sets is very small. The numbers of WV winds are larger than those of IR winds for each satellite. This difference between IR and WV winds is partly explained by the fact that the tracing target of WV winds can be selected where clouds cannot be clearly detected.

4.1.2 Wind speed dependency

Figure 3-1 shows (a) the west-east component in the Departure and (b) the histogram of the GOES-9 (MSC AMV) IR winds higher than 400 hPa over the northern hemisphere as a function of the west-east component of JRA-25 background winds. Figures 3-2 and 3-3 show the same figures, but for METEOSAT-5 and GOES-10 AMVs, respectively.

Comparing the charts (b) of Figures 3-1, 3-2 and 3-3, it can be recognized that the climatic features of wind fields over the three satellite regions are different. The magnitude of the wind speeds in the upper troposphere over the GOES-9 observation region is larger than that over the other two satellite regions. As seen in the (b) charts of Figures 3-1, 3-2 and 3-3, the absolute mean value of IR winds in the west-east component of the MSC AMV data is 17.6 m/s, whereas those for the METEOSAT-5 and GOES-10 data are 13.33 m/s and 12.21 m/s, respectively.

In the histogram of the METEOSAT-5 AMVs,

there are two peaks, as seen in Figure 3-2 (b). There are easterly winds as well as westerly winds blowing on the upper troposphere over METEOSAT-5' northern hemisphere observation region. On the other hand, Figure 3-1 (b) and Figure 3-3 (b) show that westerly winds are dominant in the upper troposphere over the MSC AMV and GOES-10 AMV northern hemisphere regions.

As seen in Figures 3-1 (a) and 3-2 (a), the Departures in MSC AMV and METEOSAT-5 AMV IR winds increase as the JRA-25 background wind speeds increase in both westerly and easterly wind ranges, except for the largest easterly wind range of the METEOSAT-5 AMV from -35 to -30 m/s. This feature indicates that slow biases are contained in both the MSC AMV and METEOSAT-5 AMVs. The biases of the GOES-10 AMVs are small over all speed ranges, except for strong easterly wind regions from -35 m/s to -20 m/s. These results are consistent with the discussion on height dependency; that is, the magnitude of the wind speed bias of GOES-10 AMV IR winds does not increase in proportion to wind speed or height.

Figure 4 shows the same figure as Figure 3, but over the southern hemisphere (60S-20S). The histogram charts (Figures 4-1, 4-2, and 4-3 (b)) show that the westerly components of IR winds over the southern hemisphere are more dominant than those over the northern hemisphere. It is considered that this situation is closely related to the seasonal differences between the northern and southern hemispheres. In addition, the absolute mean value of the MSC AMV IR winds is weaker than those of the METEOSAT-5 and GOES-10 AMVs by approximately 10 m/s. The difference between the three satellites' AMVs is partly due to the difference in land coverage. The Australian continent lies in the MSC AMV region, while on the other hand

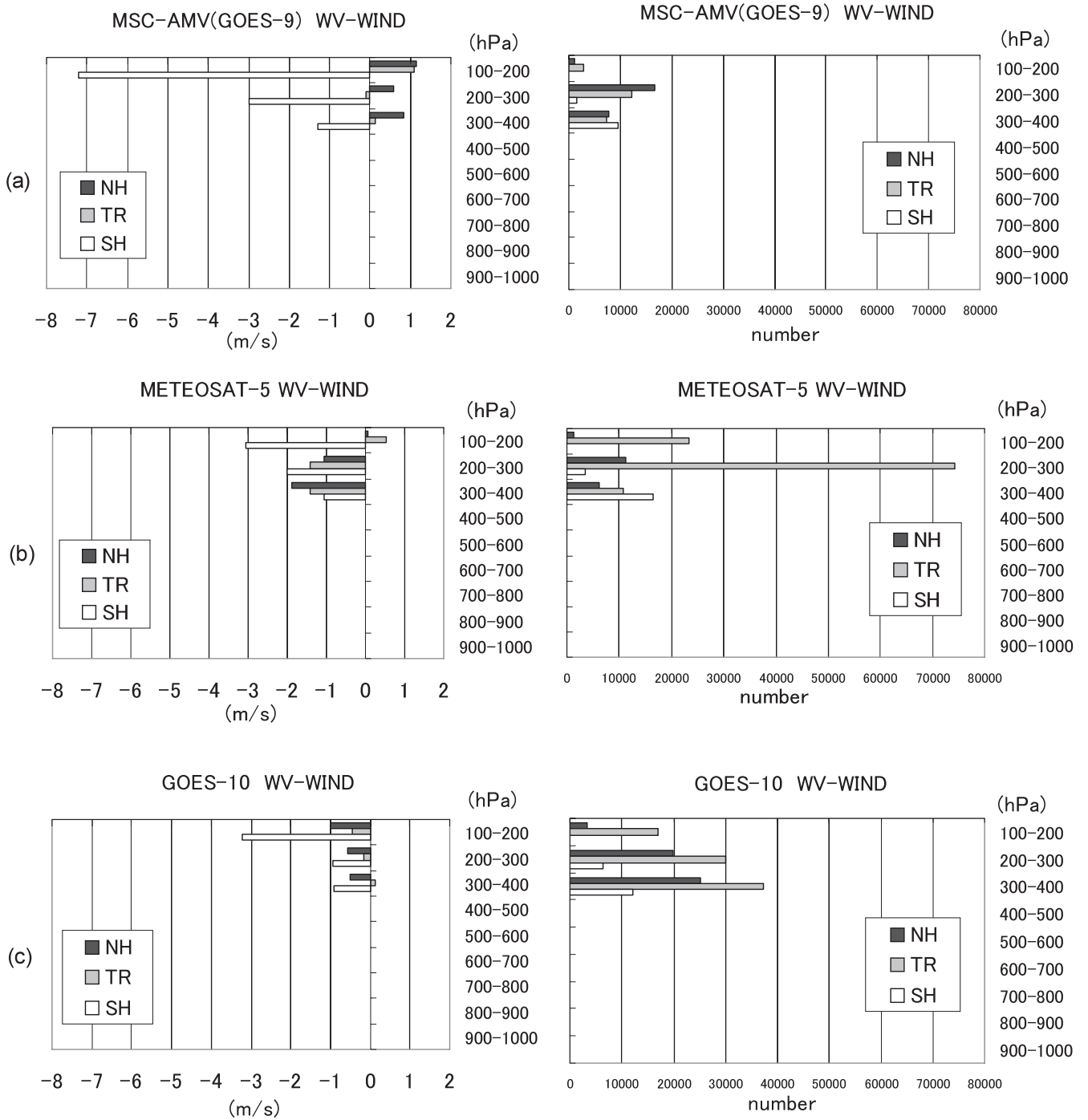


Figure 2-2: Same figure as Figure 2-1, but for WV wind.

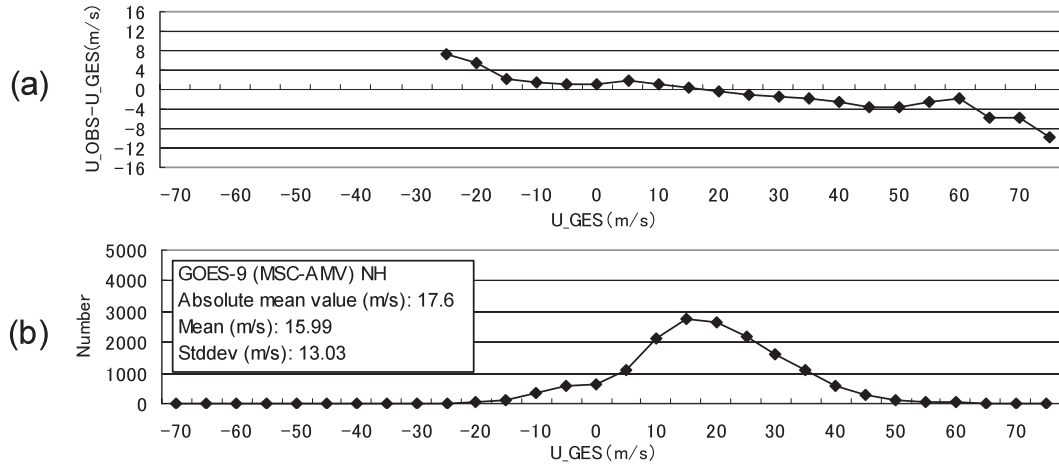


Figure 3-1: One-month averaged west-east component in (a) Departures (data minus JRA-25 first guess) and (b) one-month histogram of MSC-AMV (GOES-9) IR wind (above 400 hPa) for every 5 m/s of the first guess west-east wind component. The statistical region is the Northern hemisphere (between 20N and 60N) and the statistical month is July 2003. The absolute mean value, mean and standard deviation of the first guess west-east wind component are shown inside this figure.

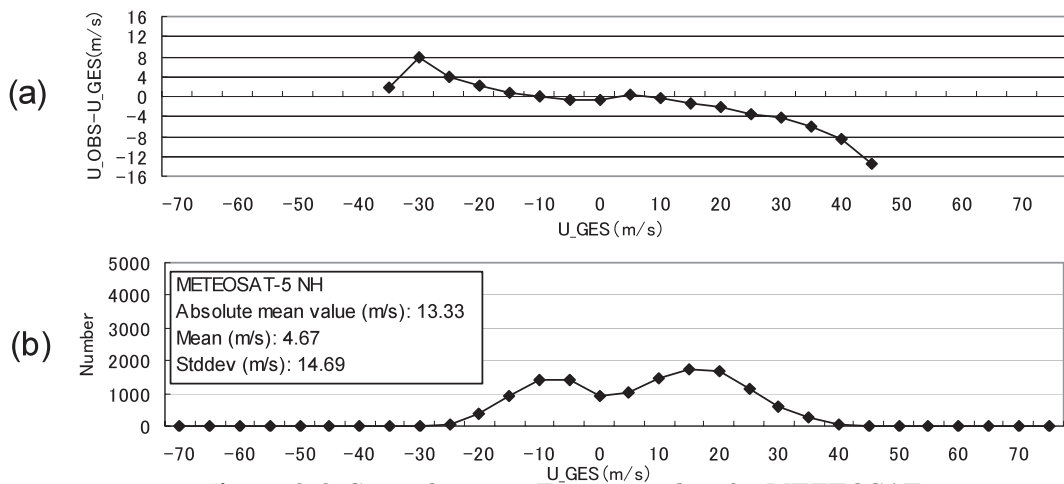


Figure 3-2: Same figure as Figure 3-1, but for METEOSAT-5.

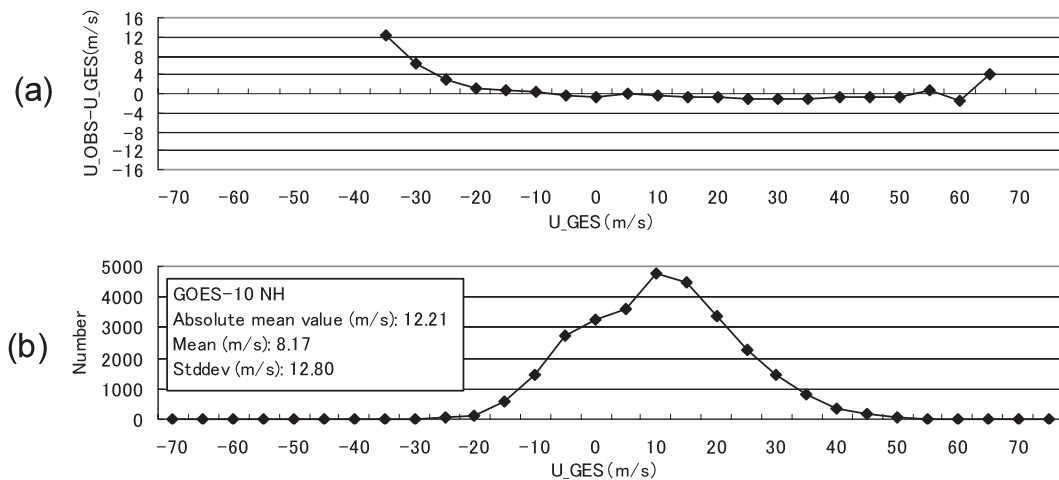


Figure 3-3: Same figure as Figure 3-1, but for GOES-10.

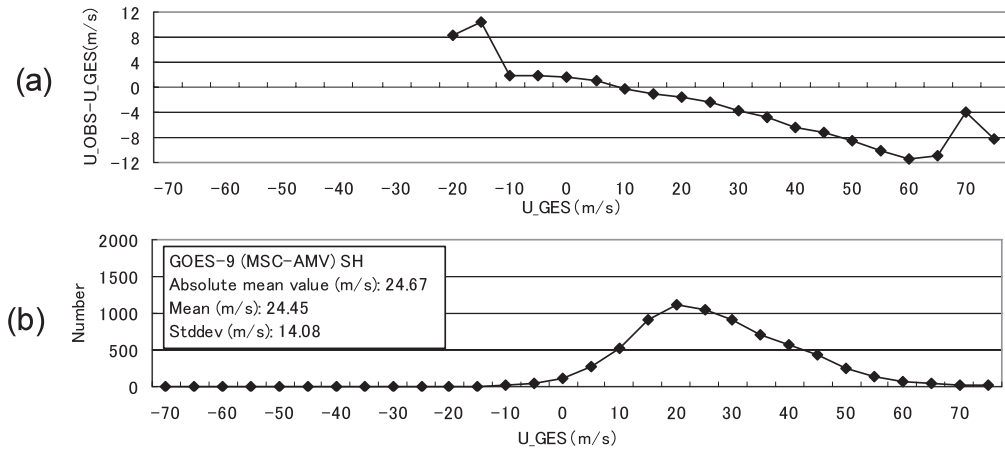


Figure 4-1: One month averaged west-east component in (a) Departures (data minus JRA-25 first guess) and one-month histogram of MSC-AMV (GOES-9) IR wind (above 400 hPa) for every 5 m/s of the first guess west-east wind component. The statistical region is the Southern hemisphere (between 60S and 20S) and the statistical month is July 2003. The absolute mean value, mean and standard deviation of the first guess west-east wind component are shown inside this figure.

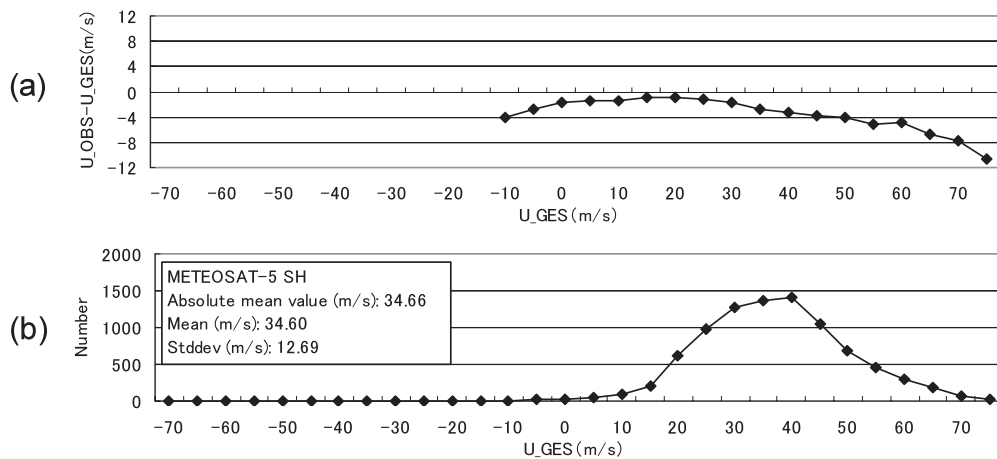


Figure 4-2: Same figure as Figure 4-1, but for METEOSAT-5.

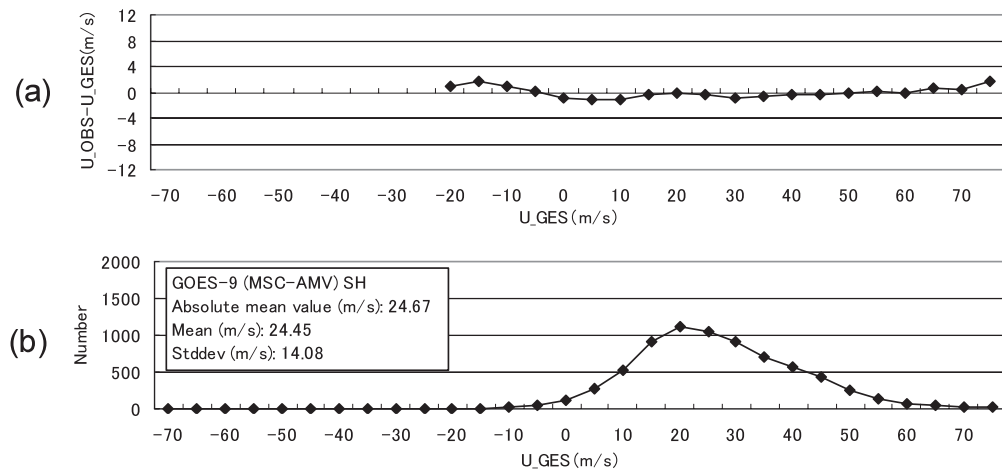


Figure 4-3: Same figure as Figure 4-1, but for GOES-10.

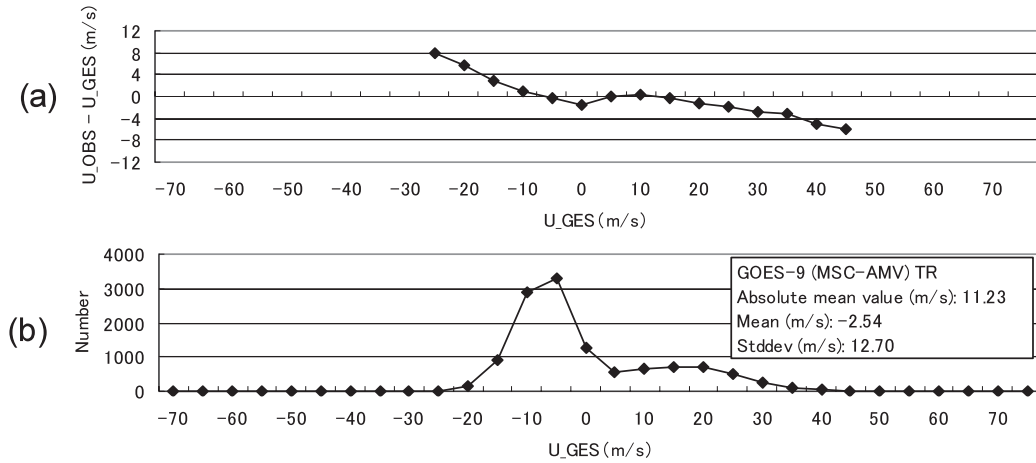


Figure 5-1: One-month averaged west-east component in (a) Departures (data minus JRA-25 first guess) and (b) one-month histogram of MSC AMV (GOES-9) IR wind (above 400 hPa) for every 5 m/s of the first guess west-east wind component. The statistical region is the Tropics (between 20S and 20N) and the statistical month is July 2003. The absolute mean value, mean and standard deviation of the first guess west-east wind component are shown inside this figure.

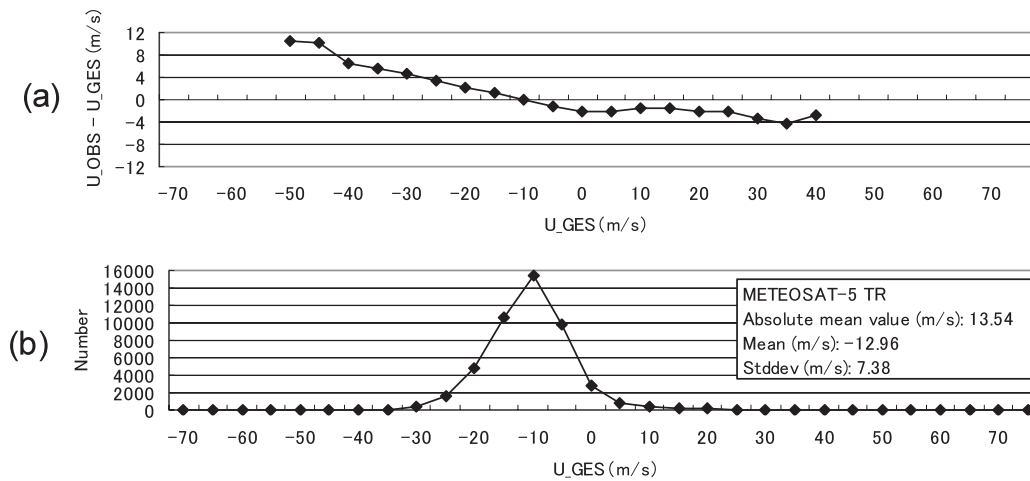


Figure 5-2: Same figure as Figure 5-1, but for METEOSAT-5.

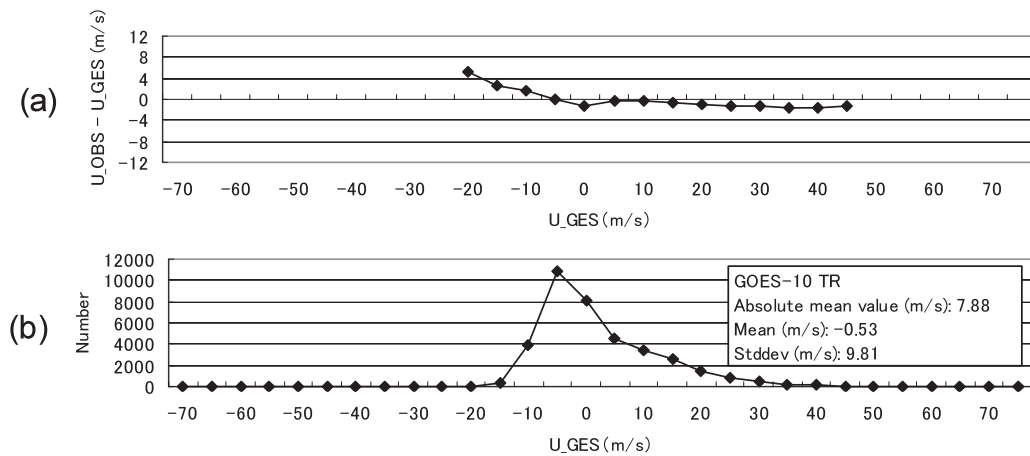


Figure 5-3: Same figure as Figure 5-1, but for GOES-10.

smaller land masses cover the other satellite AMV regions.

With respect to the Departures, the slow bias of the MSC AMV IR winds increases as the westerly component of the winds increases as seen in Figure 4-1 (a). Figure 4-2 (a) shows that the Departure in the METEOSAT AMVs also shows a similar feature to that of MSC AMVs in a westerly range. However, the easterly winds of the METEOSAT-5 AMVs are stronger than the first guess winds. As seen in Figure 4-3 (a), the Departures of the GOES-10 AMVs are very small over all speed ranges.

The speed dependency of the WV winds shows similar results to those of the IR winds over both the northern and southern hemispheres (figures are not shown). The only difference is that the west-east component of the Departure of the MSC AMVs and the METEOSAT-5 AMVs are smaller than those of their IR winds in all speed ranges. GOES-10 WV winds have much smaller slow biases than the other satellite AMVs in all speed ranges as seen in the IR wind comparison.

Figure 5 shows the same figure as Figure 3, but over the tropics. As seen in the histogram charts (Figures 5-1, 5-2 and 5-3 (b)), easterly winds are dominant over the tropics, and the ranges of the west-east component of the winds are narrower than that over the northern and southern hemispheres. The Departures in the MSC AMVs and the METEOSAT-5 AMVs indicate that the wind data contains slow biases in the easterly and westerly wind ranges as well as in the northern and southern hemispheres. The Departures in the GOES-10 AMVs are a little smaller than those over both hemispheres.

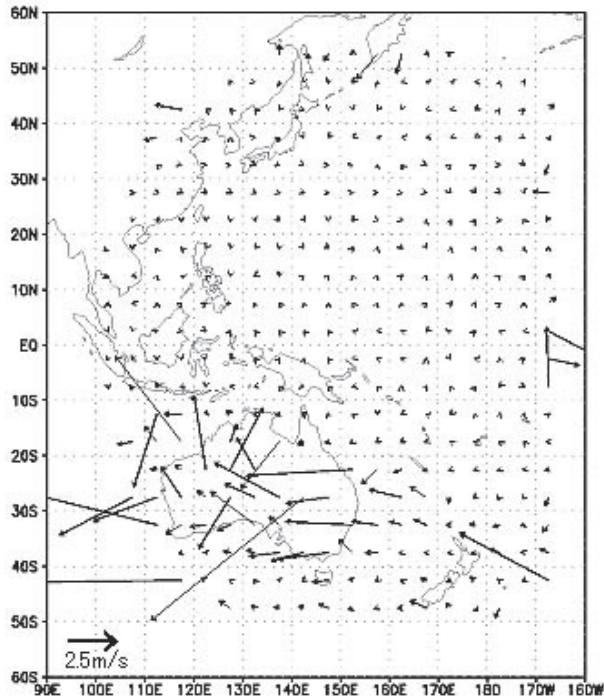
4.1.3 Spatial dependency

Figure 6 shows the spatial distributions of one-

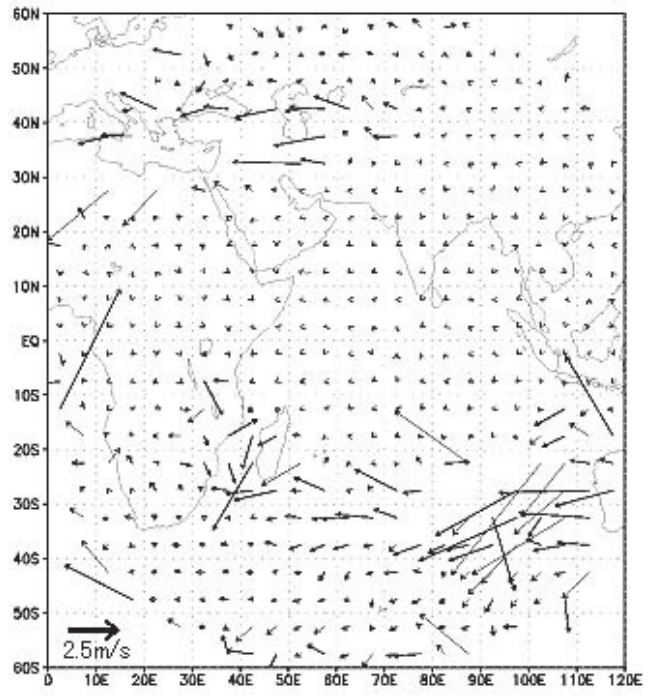
month averaged wind vector Departures between 200 and 300 hPa for (a) GOES-9 (MSC-AMV), (b) METEOSAT-5 and (c) GOES-10. The heights were chosen because the number of AMVs between these heights is generally large. With respect to MSC and METEOSAT-5 AMVs, large Departures were found from the Mediterranean Sea to the Caspian Sea and from the Australian continent to Madagascar Island. In general, one reason for obtaining the large Departures is small sampling. However, the consistent easterly Departures indicate that the slow biases of the MSC and METEOSAT-5 AMVs appeared over these regions. One of the reasons for the slow speed biases is the difficulty of height assignment and the tracing of AMVs over land, because radiance from the land surface prevents AMVs from the normal retrieval. However, the reasons are unclear here because slow biases do not always appear over land. As for the speed bias at around 90E and 30S near the Australian continent, it appears over the ocean. The reason is not clear for the complicated distribution of several types of clouds. The Departures in the GOES-10 AMVs are small over the entire domain. The small Departure credits the bias adjustment applied to the GOES-10 AMVs.

4.2 Impact of the AMVs in July 2003

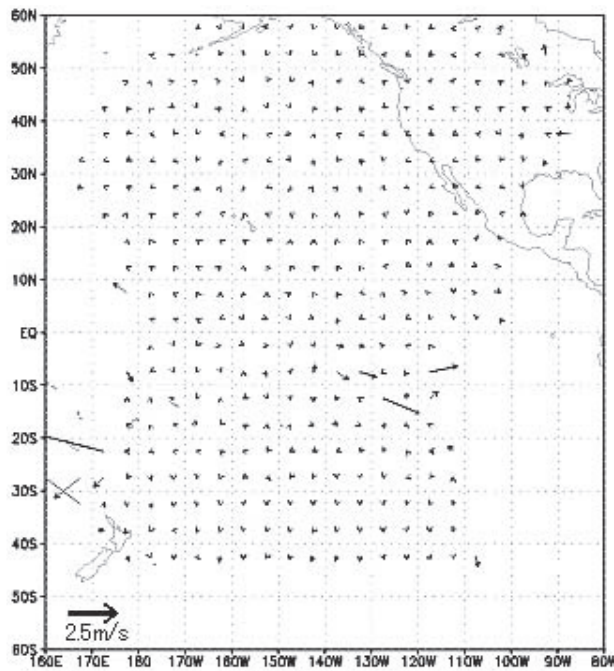
In order to evaluate the impact of AMV data on the JRA-25 analysis fields, the OSEs were examined. The control run (CTRL) is equivalent to the JRA-25 official run, where all AMV data was assimilated. Only the METEOSAT-5 and 7 AMVs were assimilated using the QI criteria shown in Table 2. Three experimental runs (TEST1, 2, and 3) were examined by removing some or all of the AMV data from CTRL. Table 3 shows the difference between the test runs and the control run. The



(a) GOES-9 (MSC-AMV)



(b) METEOSAT-5



(c) GOES-10

Figure 6: The spatial distributions of the Departures (data minus JRA-25 first guess) of each satellite's AMVs (IR and WV winds) between 200 and 300 hPa. The departures are shown by vectors whose west-east and south-north components are averaged over 5-degree latitude/longitude boxes. (a) GOES-9 (MSC AMVs), (b) METEOSAT-5 and (c) GOES-10. The statistical month is July 2003.

Table 3: The configuration of experiments Test1, Test2, Test3 and CTRL

Experiment Name	TEST1	TEST2	TEST3	CTRL
Period	July 2003			
Upper Layer AMV (Above 400 hPa height)	None	Used	None	Used
Middle Layer AMV (700 hPa to 400 hPa height)	Used	Used	None	Used
Lower Layer AMV (below 700 hPa height)	Used	None	None	Used

settings shown in Table 3 are equally applied to all satellite AMVs. The experimental period is from 00 UTC July 1st to 18 UTC July 31st in 2003. First guess fields used in the first analysis of the test runs were the same as those of the control runs. To investigate the impact of AMV data, one-month averaged analysis fields were evaluated.

4.2.1 Impacts of upper tropospheric AMVs on the wind field

Figure 7 shows (a) the one-month averaged analysis wind field of CTRL at 300 hPa and (b) the difference between CTRL and TEST1 which is an experimental run by subtracting AMV data higher than 400 hPa from CTRL.

In Figure 7 (b), the differences are relatively small over the middle latitude of the northern and southern hemispheres, whereas large vector Departures are seen in Figures 6 (a) and (b). These results show that the influence of the slow bias of each satellite's AMVs over the upper troposphere, which is shown in 4.1.1, 4.1.2 and 4.1.3, is fortunately avoided to some extent. However, slow biases of 1-2 m/s can be recognized over 50S-40S of METEOSAT-5's observation region. Over the tropics, large differences can be recognized in some regions.

Figures 7 (a) and (b) show that the easterly

winds over the Equator in the Indian Ocean are strengthened by assimilating the upper tropospheric AMV data. The easterly winds arise from the Indian monsoon system. Over the sea off Peru in the tropical eastern Pacific Ocean, the north-south exchange of kinetic momentum is intensified between the upper tropospheric easterly and westerly winds through the increase in the north-south wind component. Over the tropical Atlantic Ocean, westerly and easterly winds between 20S and 10N are strengthened by the assimilation of the upper tropospheric AMVs.

The largest impact can be recognized over the tropical Indian Ocean. Figure 8 shows the spatial distributions of the one-month averaged wind vector Departures (data minus first guess) between 300 and 400 hPa for the METEOSAT-5 AMVs. Large easterly Departures can be recognized between 5N and 15N. This feature is not seen between 200 and 300 hPa in Figure 6 (b). The Departures seem to correspond to the impact over the tropical Indian Ocean. However, Figure 7 (b) shows that the large easterly wind difference between CTRL and TEST1 is located slightly to the south, between 15S and 10N. The anticlockwise wind circulation located there is strengthened by the assimilation of upper tropospheric AMVs.

Figure 9 (a) shows the difference in horizontal

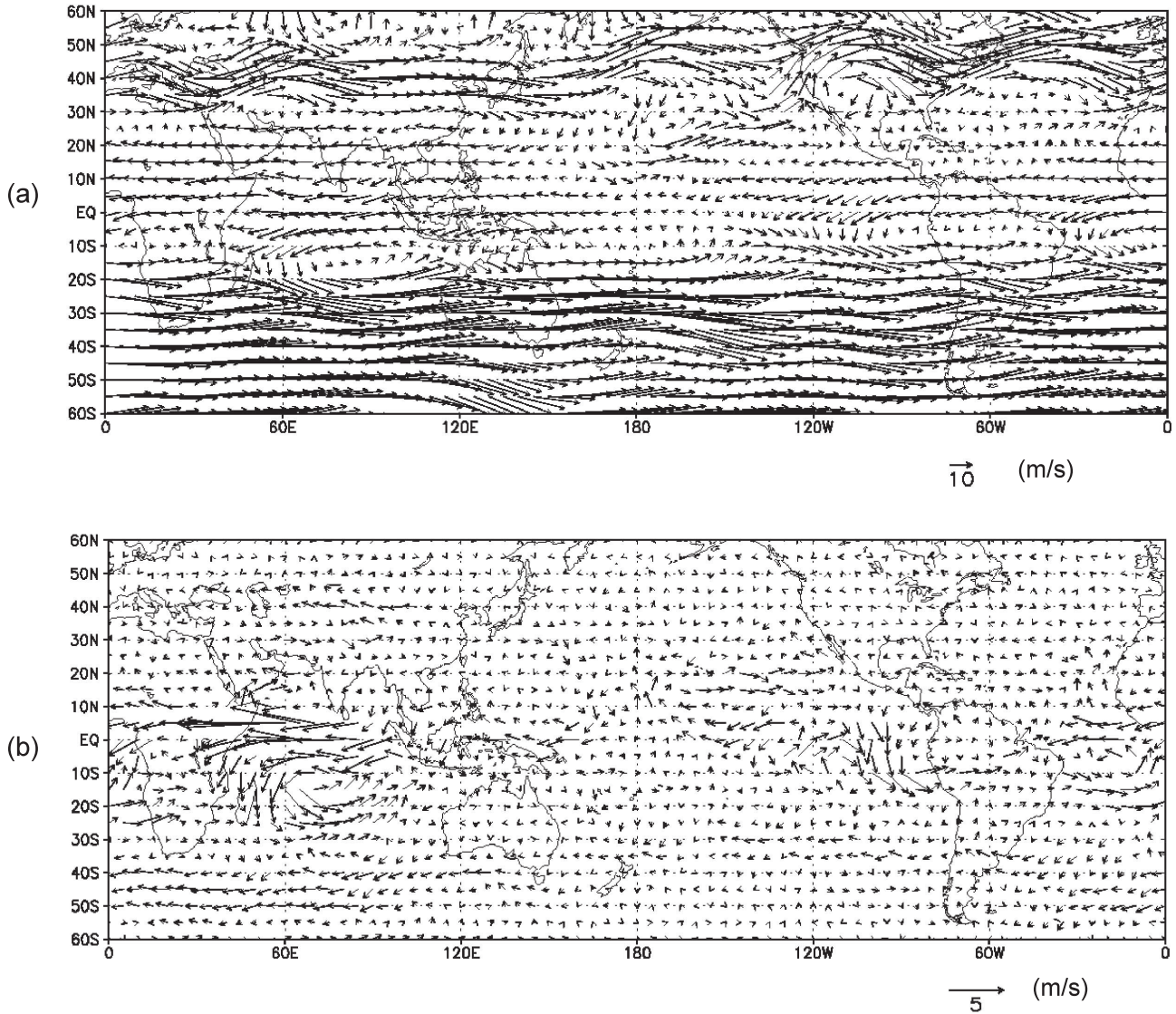


Figure 7: (a) One-month averaged analysis wind vectors (m/s) at 300 hPa for CTRL, (b) the difference in the one-month averaged analysis wind vectors (m/s) at 300 hPa height between CTRL and TEST1. The westerly vector shown in Figure 7 (b) means that the westerly (easterly) wind of CTRL is stronger (weaker) than that of TEST1. The statistical month for (a) and (b) is July 2003.

divergence fields at 200 hPa between CTRL and TEST1. The large impact recognized over the Indian Ocean also affects the upper tropospheric divergence field around the region. In particular, the large positive difference, that indicates the increase in divergence by the AMVs, is found from 65E to 80E and 15S to the Equator.

Figure 9 (b) shows the same figure as Figure 9 (a), but at 850 hPa. The large modifications in the

divergence field can be recognized at 850 hPa as well as at 200 hPa. Analyzing the vertical cross-section of rotation fields (the figure is not shown), the modification of the upper tropospheric horizontal circulation is conveyed to the middle and lower troposphere, through the sinking of the upper tropospheric horizontal circulations in the cyclic analysis and forecast schemes. An exceptional feature can be recognized from the Equator to 10N

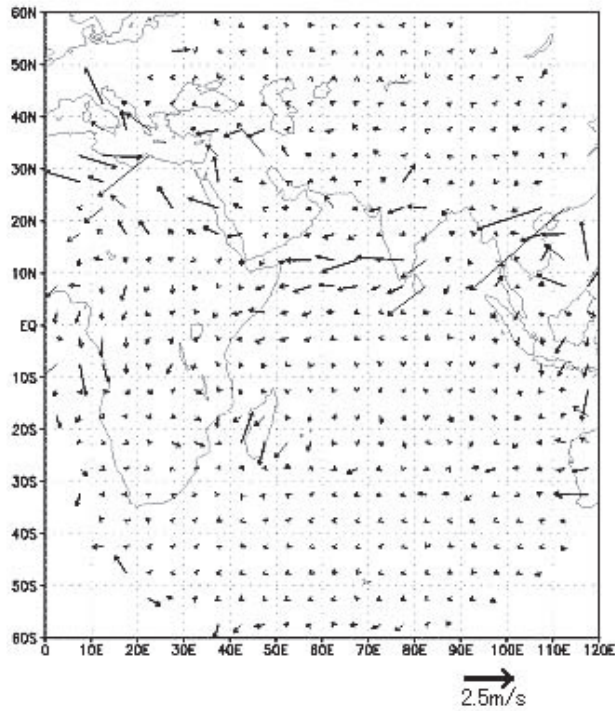


Figure 8: The spatial distribution of Departures (data minus JRA-25 first guess) of METEOSAT-5 AMVs (IR and WV winds) between 300 and 400 hPa. The departures are shown by vectors whose west-east and south-north components are averaged over 5-degree latitude/longitude boxes. The westerly vector shown in Figure 8 means that the westerly (easterly) wind of the AMVs is stronger (weaker) than that of the first guess. The same region as Figure 6 (b) is shown. The statistical month is July 2003.

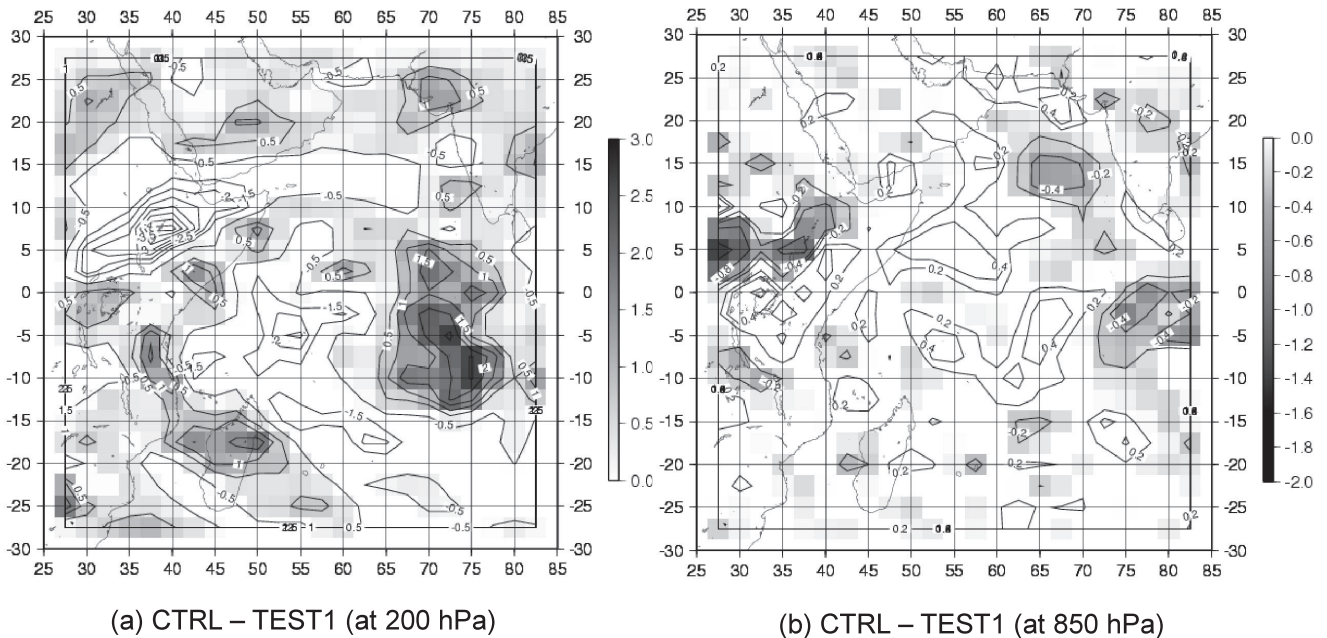


Figure 9: The difference in the one-month averaged divergence analysis fields ($10^{-6}/s$) at (a) 200 hPa and (b) 850 hPa between CTRL and TEST1 over the tropical Indian Ocean (30S-30N and 25E-85E). Positive values mean that the divergence of CTRL is larger than that of TEST1. The negative values in Figure 9 (a) and positive values in Figure 9 (b) are not shaded, respectively. The statistical month of (a) and (b) is July 2003.

and from 30E to 40E; that is, the intensification of upper tropospheric divergence does not correspond to that of the lower tropospheric convergence. The reason is not clear.

4.2.2 Impacts of lower tropospheric AMVs on the wind field

Figure 10 (a) shows the one-month averaged analysis wind field at 850 hPa of CTRL. Figure 10

(b) shows the difference in the one-month averaged analysis wind field at 850 hPa between CTRL and TEST2 which is an experimental run by subtracting AMVs lower than 700 hPa from CTRL.

A large impact can be recognized over the tropical eastern Pacific Ocean which is located inside the GOES-10 and 12 observation range. A clockwise circulating wind impact can be recognized there by assimilating the lower tropospheric AMV data. Also,

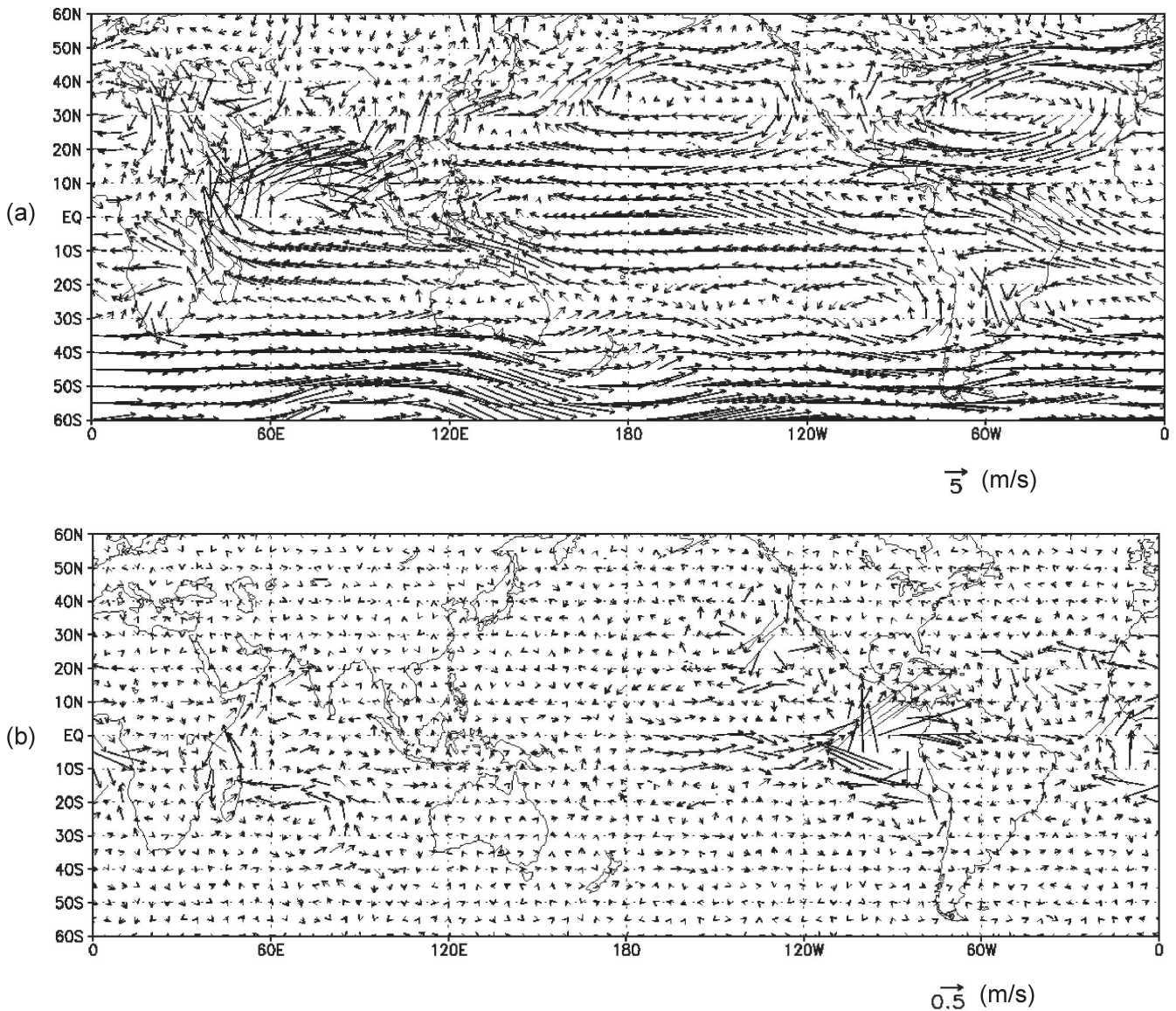


Figure 10: (a) One-month averaged analysis wind vectors (m/s) at 850 hPa for CTRL, (b) the difference in one-month averaged analysis wind vectors (m/s) at 850 hPa between CTRL and TEST2. The westerly vector shown in Figure 10 (b) means that the westerly (easterly) wind of CTRL is stronger (weaker) than that of TEST2. The statistical month for (a) and (b) is July 2003.

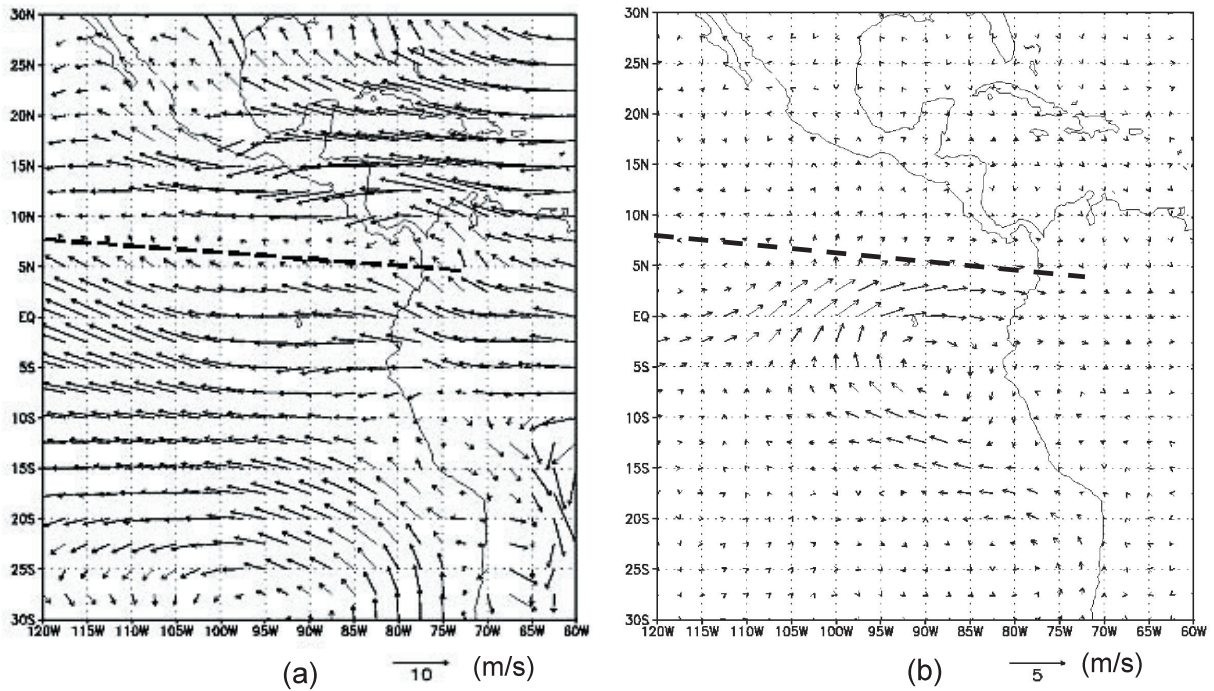


Figure 11: (a) One-month averaged analysis wind vectors (m/s) at 850 hPa for CTRL, (b) the difference in one-month averaged wind analysis vectors (m/s) between CTRL and TEST2. The westerly vector shown in Figure 11 (b) means that the westerly (easterly) wind of CTRL is stronger (weaker) than that of TEST2. The region is the tropical eastern Pacific Ocean (30S-30N and 120W-60W). The broken lines show horizontal shear lines by analyzing the wind field of CTRL. The statistical month of (a) and (b) is July 2003.

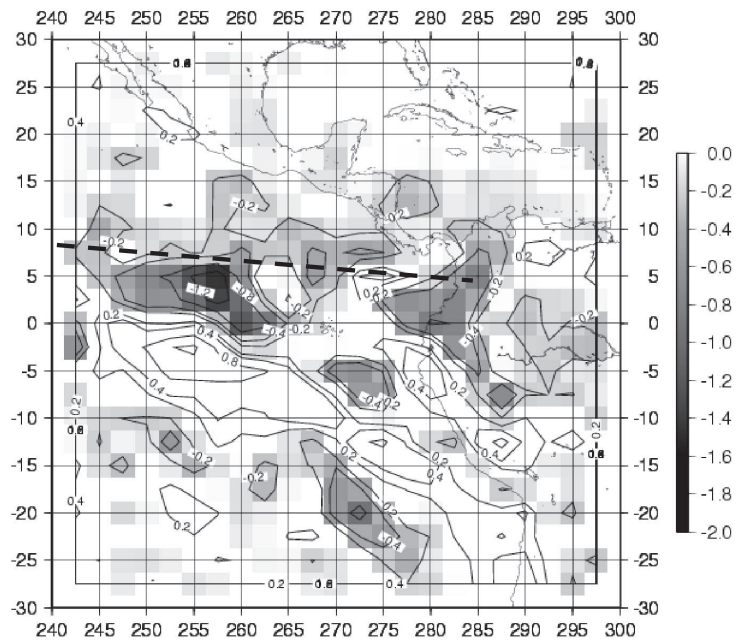


Figure 12: The difference in one-month averaged divergence analysis fields ($10^{-6}/s$) at 850 hPa between CTRL and TEST2 over the tropical eastern Pacific Ocean (30S-30N and 120W-60W). A negative value means that the convergence of CTRL is larger than that of TEST2. Positive values are not shaded. The broken lines show horizontal shear lines by analyzing the wind field of CTRL. The statistical month is July 2003.

easterly winds are weakened from 170W to 120W over the tropical Pacific Ocean. This impact seems to correspond to the positive Departure in the west-east wind component below 800 hPa over the tropics of the GOES-10 observation range which is seen in Figure 2-1 (c). In the tropical eastern Atlantic Ocean, a similar clockwise circulation is strengthened between 20S and 10N.

Figures 11 (a) and (b) show the same figures as Figures 10 (a) and (b), respectively, but the region is over the tropical eastern Pacific Ocean, where the largest impact was found. The wind shear is recognized along the Intertropical Convergence Zone (ITCZ). The clockwise circulating modification is located just to the south. Figure 12 shows the difference in the divergence fields at 850 hPa between CTRL and TEST2. It can be recognized that the lower tropospheric convergence corresponding to ITCZ is strengthened between 5S and 15N.

For the other impacts, Figure 10 (b) shows that the northeastern winds over the northeastern Pacific Ocean seen in Figure 10 (a) are strengthened by the assimilation of the lower tropospheric AMVs. This region is located to the southeast of the clockwise wind circulation arising from subtropical high pressure.

Meanwhile, over the tropics and subtropical region of the Indian Ocean, the lower tropospheric clockwise circulation arising from the Indian monsoon system is strengthened. This impact leads to an increase of lower tropospheric warm and humid inflow over the region.

4.2.3 Impacts of all AMVs on the wind field

In this section, the impacts of all AMV data on the JRA-25 wind field are examined. Figure 13-1 (a) shows the differences of the one-month averaged

analysis wind field at 300 hPa between CTRL and TEST3 which is an experimental run by subtracting all AMVs from CTRL.

With respect to the impacts on the wind field at 300 hPa, the vector differences between Figure 13-1 (a) and Figure 7 (b) is small. For an example of the similarity, the strengthening of easterly winds over the tropical Indian Ocean and anti-clockwise circulation over the subtropical region of the Indian Ocean can be commonly recognized in both figures. This shows that the wind field at 300 hPa is hardly affected by AMVs lower than 400 hPa.

Figure 13-1 (b) shows the difference in one-month averaged analysis wind vectors at 300 hPa between TEST1 and TEST3. The large vector differences in Figure 13-1 (b) mean that the impact of AMVs below 400 hPa on the wind field at 300 hPa is large. Over the eastern tropical Pacific Ocean (inside the solid circle in Figure 13-1 (b)), an anticlockwise circulating impact can be recognized. This feature indicates that the assimilation of AMVs on the middle and lower troposphere affects the upper tropospheric wind field over the region. However, it is difficult to account for the effect on the upper tropospheric wind field because the contributions of the respective satellites' AMVs need to be considered.

With respect to the impact on the wind field at 850 hPa, the vector differences between Figure 13-2 (a) and Figure 10 (b) is small. For an example of the similarity, distinct impacts over the eastern tropical Pacific Ocean can be seen in both figures. This feature shows that the impacts on the wind field at 850 hPa are hardly affected by AMVs above 700 hPa.

Figure 13-2 (b) shows the difference in the one-month averaged analysis wind vectors at 850 hPa between TEST2 and TEST3. The large vector differences in Figure 13-2 (b) mean that the impact

of AMVs above 700 hPa on the wind field at 850 hPa is large. There are some large vector differences over the middle of Africa, the tropics of the Indian Ocean, the tropical western Pacific Ocean, the sea off Peru and the north of South America (inside the solid circles in Figure 13-2 (b)). These features indicate

that the assimilation of AMVs in the upper and middle troposphere affects the lower tropospheric wind field over the regions.

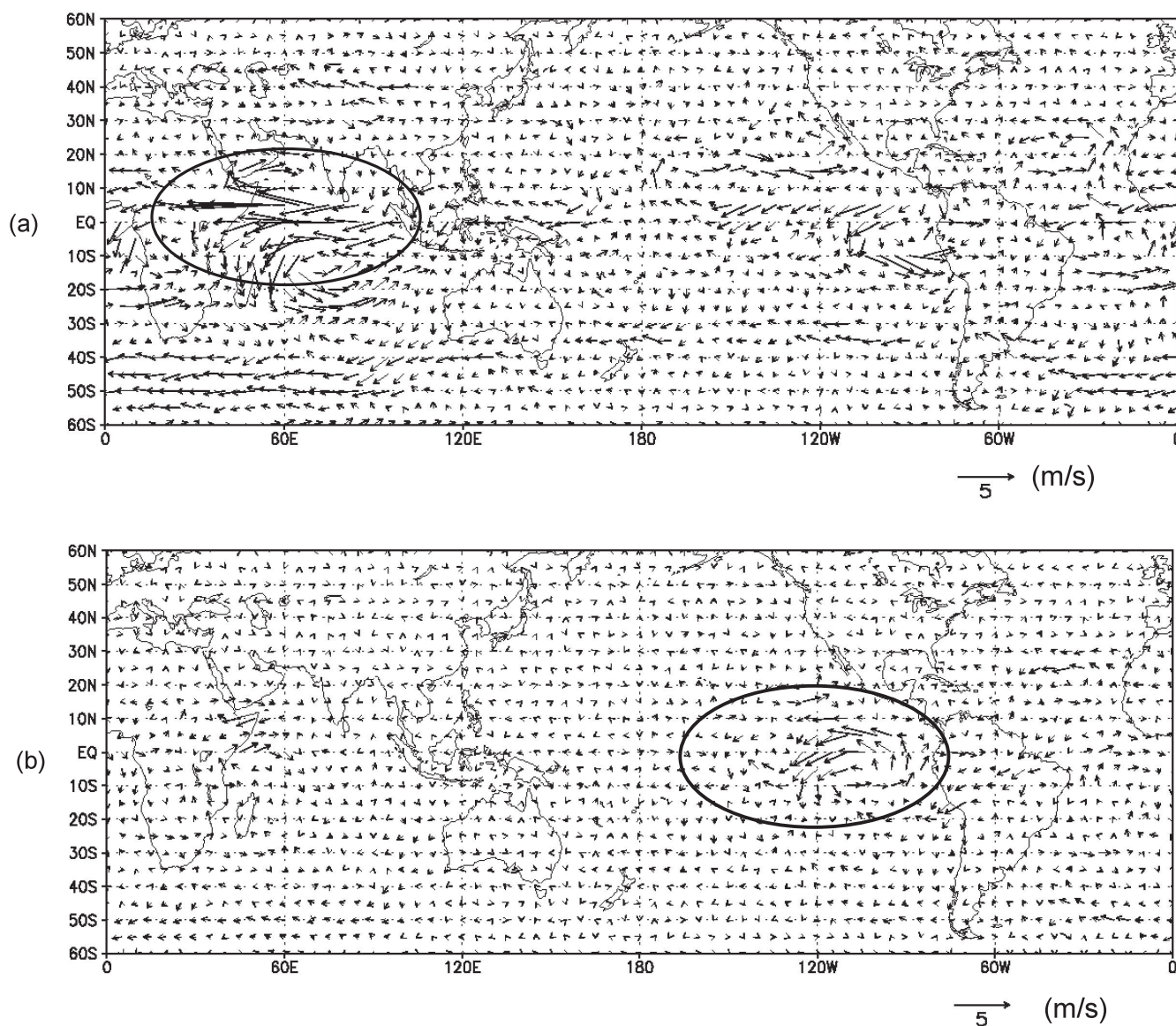


Figure 13-1: (a) The difference in one-month averaged analysis wind vectors (m/s) at 300 hPa between CTRL and TEST3. The westerly vector means that the westerly (easterly) wind of CTRL is stronger (weaker) than that of TEST3. The circle in Figure 13-1 (a) shows the location of the wind impact referred to in section 4.2.3. (b) The difference in one-month averaged analysis wind vectors (m/s) at 300 hPa between TEST1 and TEST3. The circle in Figure 13-1 (b) shows the larger vector differences between TEST1 and TEST3 referred to in section 4.2.3. The statistical month of (a) and (b) is July 2003.

4.2.4 Impacts of all AMV on the precipitation field

In 4.2.1, 4.2.2 and 4.2.3, it is shown that the assimilation of AMVs effectively modifies not only the wind field, but also the horizontal divergence

field in the upper and lower troposphere over the tropics. It is considered that these modifications also affect the precipitation field over the regions. To verify the contributions of the upper and lower tropospheric AMV data to the JRA-25 precipitation

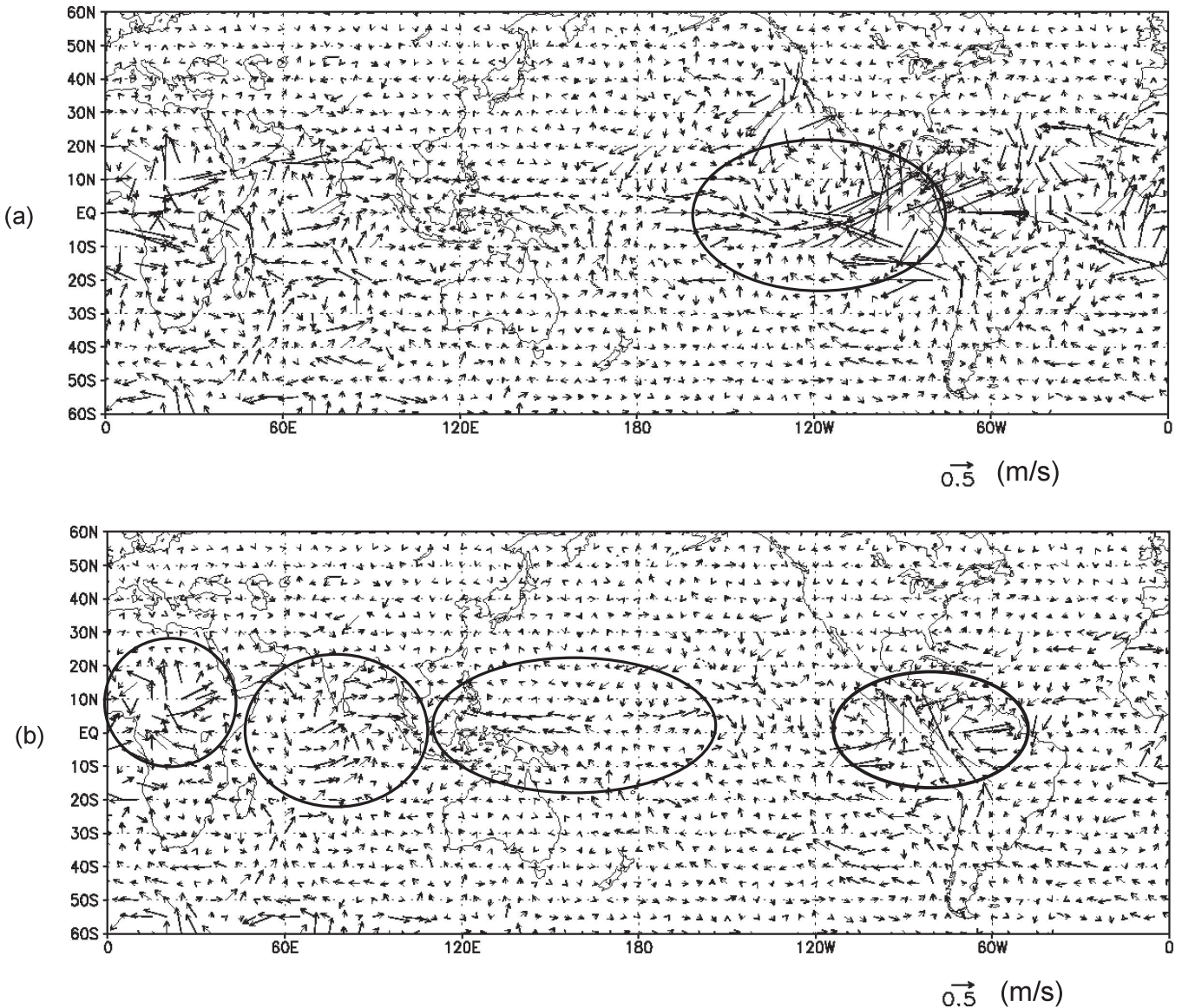


Figure 13-2: (a) The difference in one-month averaged analysis wind vectors (m/s) at 850 hPa between CTRL and TEST3. The westerly vector means that the westerly (easterly) wind of CTRL is stronger (weaker) than that of TEST3. The circle in Figure 13-2 (a) shows the location of the wind impact referred to in section 4.2.3. (b) The difference in one-month averaged analysis wind vectors (m/s) at 850 hPa between TEST2 and TEST3. The circles in Figure 13-2 (b) show the larger vector differences between TEST2 and TEST3 referred to in section 4.2.3. The statistical month of (a) and (b) is July 2003.

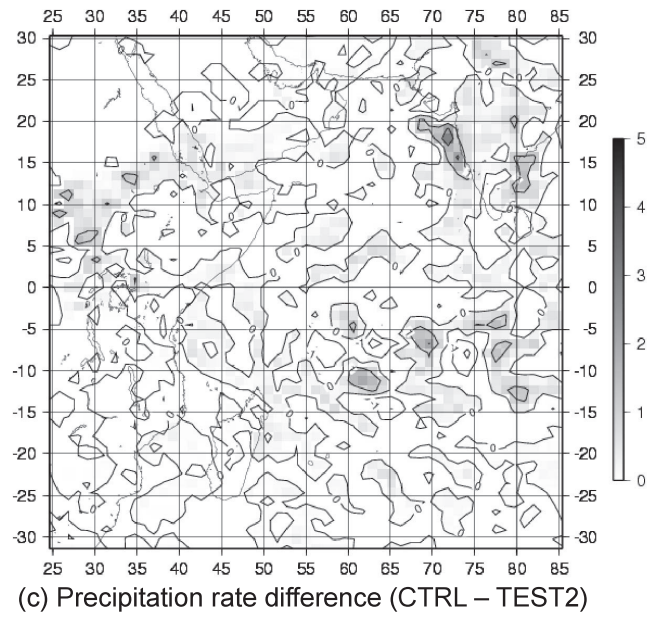
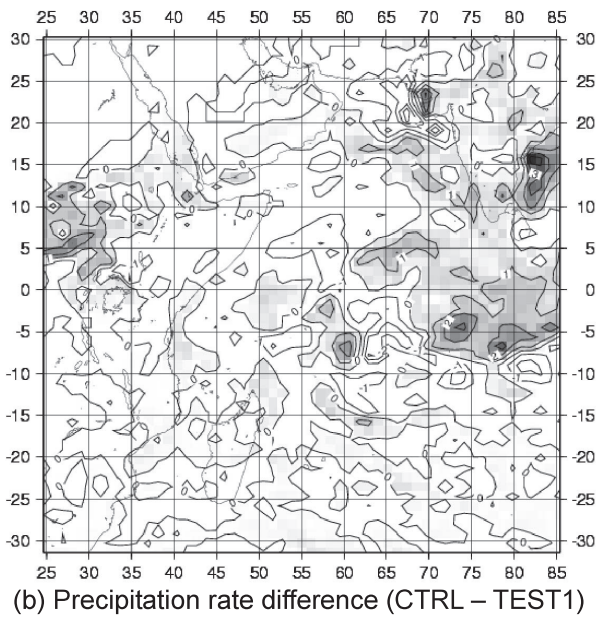
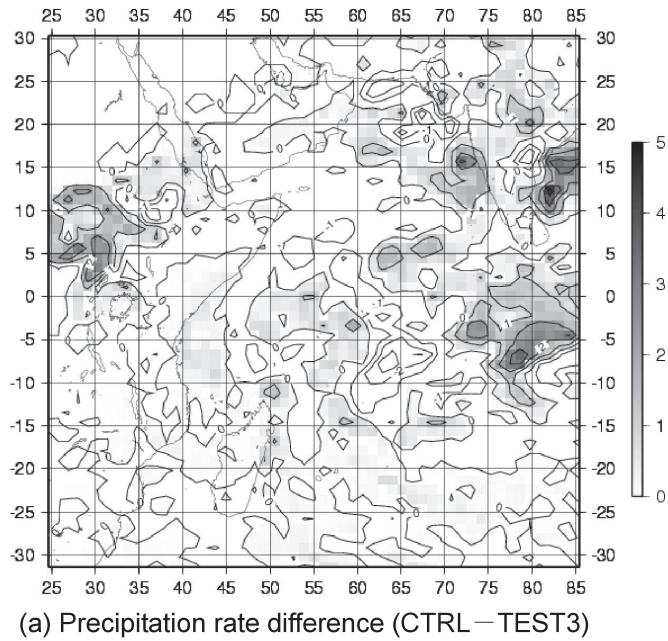


Figure 14: The differences in one-month averaged precipitation rate (mm/day) (a) between CTRL and TEST3, (b) CTRL and TEST1, and (c) CTRL and TEST2 over the tropical Indian Ocean (30S-30N and 25E-85E). A positive value means that the precipitation rate of CTRL is larger than that of TEST. Negative values in this figure are not shaded. The statistical month of (a), (b) and (c) is July 2003.

field, TEST1, TEST2 and TEST3 are examined.

Figures 14 (a), (b), and (c) show the differences in the precipitation rate over the tropical Indian Ocean between CTRL and TEST3, CTRL and TEST1, and CTRL and TEST2, respectively. Figure 14 (c) shows that the precipitation difference between CTRL and TEST2 is small, whereas a large difference between CTRL and TEST1 can be recognized in Figure 14 (b). Comparing Figure 14 (b) and Figure 9 (b) showing the difference in the divergence fields at 850 hPa between CTRL and TEST1, the increases in the precipitation in Figure 14 (b) closely correspond to the increase in the convergence. Figure 14 (a) is more similar to Figure 14 (b) than Figure 14 (c) on the basis of distribution and magnitude, except for the west coast of India. Hence, this result shows that the contribution of the upper tropospheric AMVs on the JRA-25 precipitation field is larger than that of the lower tropospheric AMVs over the tropical Indian Ocean.

Figure 15 is the same figure as Figure 14, but for the tropical eastern Pacific Ocean. The broken lines (horizontal shear line) are drawn to the south of the ITCZ precipitation band. Even though the large increase in convergence just to the south of the broken line by assimilating the lower tropospheric AMVs can be recognized in Figure 12, Figure 15 (c) shows that the precipitation increase is located just to the north of the line and the decrease is to the south. Figure 15 (b) also shows that the precipitation increases by assimilating the upper tropospheric AMVs are located to the north of the line. It seems that the impacts on the precipitation field seen in TEST3 are the combination of the impacts observed in TEST1 and TEST2.

4.2.5 Precipitation evaluation by CMAP data for July 2003

To evaluate the effectiveness of the AMVs on the precipitation field over the tropical Indian Ocean and the tropical eastern Pacific Ocean, the precipitation fields are compared with the Climate Prediction Center (CPC) Merged Analysis Precipitation (CMAP) data. The CMAP data is precipitation data incorporating estimated precipitation rates retrieved from satellite data, such as GOES, SSM/I, the NOAA Advanced Very High Resolution Radiometer (AVHRR) and the Microwave Sounding Unit (MSU) (Gruber et al., 2000).

Figure 16 (a) and (b) show the differences in the one-month averaged precipitation rate between CTRL and CMAP, and TEST3 and CMAP, respectively. Positive value in these figures shows that the precipitation rate of CTRL or TEST3 is larger than that of CMAP. The difference between Figure 16(a) and (b) is small. However, it can be recognized that the difference between CTRL and CMAP is larger than that between TEST3 and CMAP at around (0, 80E), (20N, 75E), and (10N, 35E). On the other hand, the difference between CTRL and CMAP is smaller than that between TEST3 and CMAP over northwest India, from 10S to the Equator and from 65E to 70E.

Figure 16 also shows (c) the one-month averaged precipitation rate of CMAP data and (d) the difference between CTRL and TEST3 of the absolute values of the one-month averaged precipitation rate residuals from CMAP over the tropical Indian Ocean. The differences seen in Figure 16 (d) are small over the region. However, large positive differences can be recognized around (0, 83E), (20N, 75E), and (10N, 33E). This feature means that the quantity of the precipitation in CTRL is more divergent from CMAP than that in TEST3.

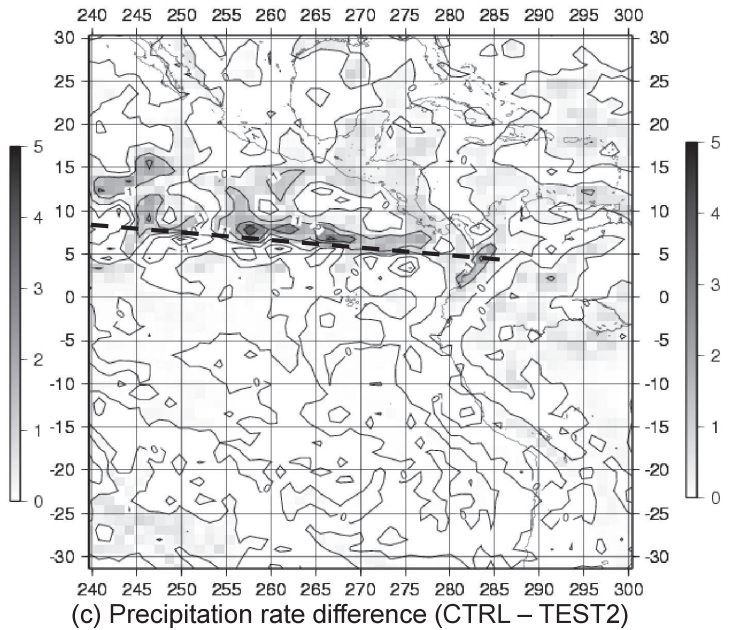
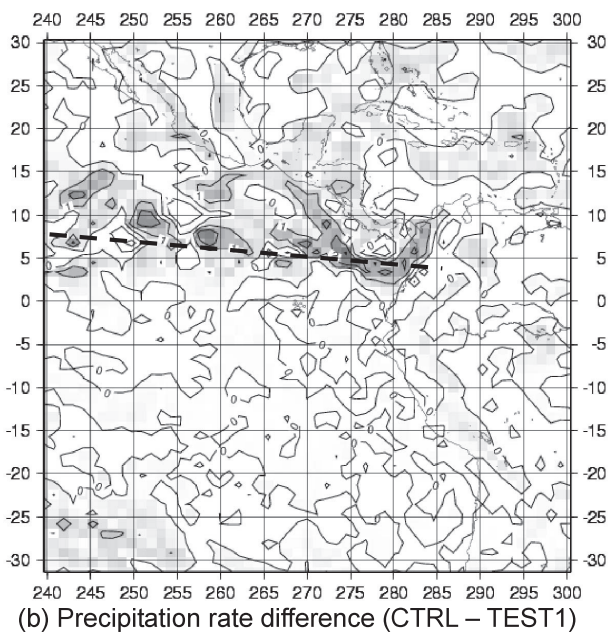
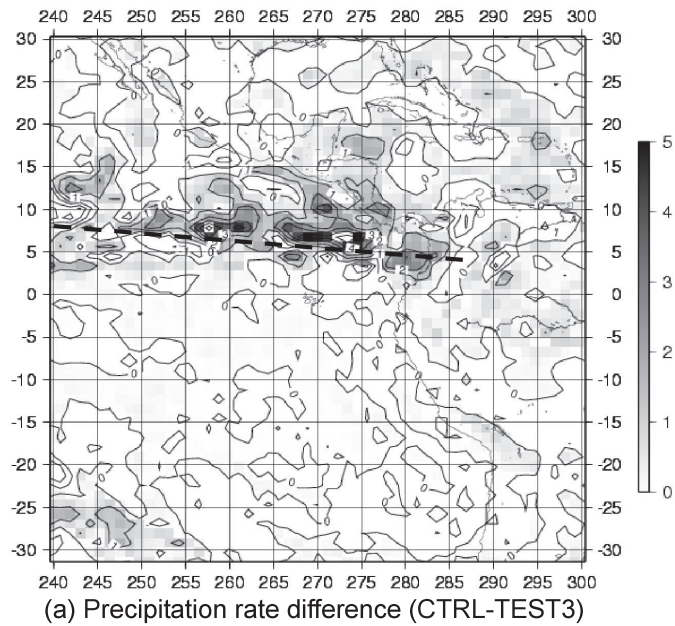


Figure 15: The differences in one-month averaged precipitation rate (mm/day) (a) between CTRL and TEST3, (b) CTRL and TEST1, and (c) CTRL and TEST2 over the tropical eastern Pacific Ocean (30S-30N and 120W-60W). A positive value means that the precipitation rate of CTRL is larger than that of TEST. Negative values are not shaded. The broken line shows the horizontal shear line by analyzing the wind field of CTRL. The statistical month of (a), (b) and (c) is July 2003.

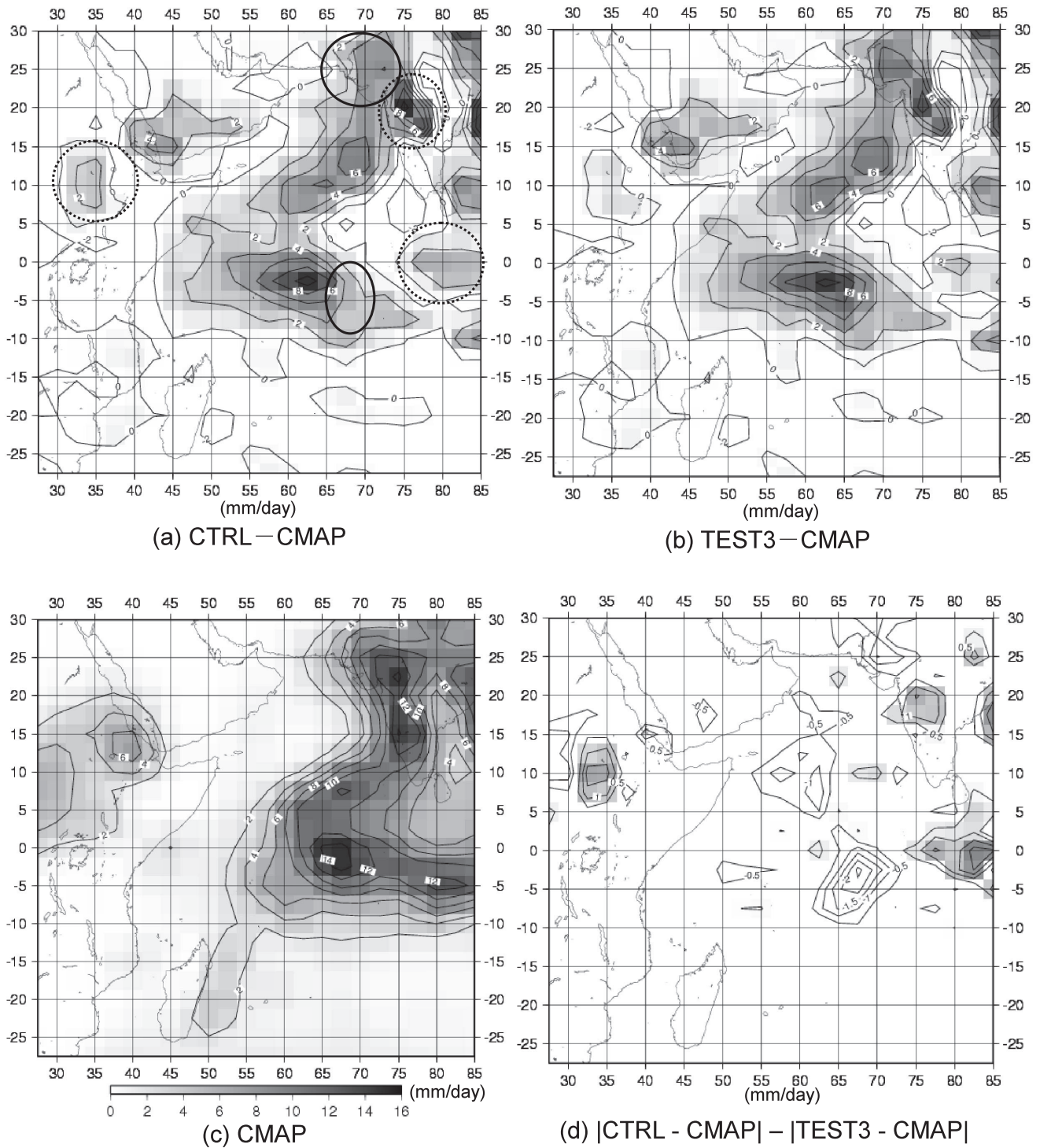


Figure 16: The differences in one-month averaged precipitation rate (a) between CTRL and CMAP, (b) between TEST3 and CMAP, (c) one-month averaged precipitation rate of CMAP data, and (d) the difference between CTRL and TEST3 of the absolute values of the one-month averaged precipitation rate residuals from CMAP. The solid circles in Figure 16 (a) show where the precipitation rate of CMAP data is closer to that of CTRL than TEST3, and the dotted circles show the opposite. Positive (negative) values in figure 16 (d) show the areas where the differences in the precipitation rate between CTRL and CMAP is larger (smaller) than that between TEST3 and CMAP. Negative values in Figure 16 (a) - (d) are not shaded. The region is over the tropical Indian Ocean (30S-30N and 25E-85E). The statistical month of (a) - (d) is July 2003.

Table 4: One-month statistical precipitation evaluations of CTRL and TEST3 with CMAP data for (a) the Indian Ocean and (b) the tropical eastern Pacific Ocean. Correlation, root mean square error (RMSE) and mean difference (MD) are shown. The statistical month is July 2003.

(a) Tropical Indian Ocean (30S–30N and 25E–85E)

July 2003		CTRL(use AMV)	TEST3 (use no AMV)
	Correlation	0.91	0.91
	RMSE(mm/day)	2.37	2.41
	MD(mm/day)	0.84	0.83

(b) Tropical Eastern Pacific Ocean (30S–30N and 120W–60W)

July 2003		CTRL(use AMV)	TEST3 (use no AMV)
	Correlation	0.84	0.83
	RMSE(mm/day)	3.16	3.03
	MD(mm/day)	1.18	1.08

These positions correspond to where the positive differences of precipitation rates between CTRL and TEST3 can be found in Figure 14 (a). On the other hand, the differences in Figure 16 (d) are negative around (3S, 67E), (25N, 70E), and (10N, 60E).

Table 4 (a) shows the correlation, root mean square error (RMSE) and mean difference (MD) between CTRL and CMAP, and TEST3 and CMAP over the tropical Indian Ocean (30S - 30N and 25E - 85E). The AMV impacts over the tropical Indian Ocean are almost neutral, but small shifts in precipitation can be recognized.

Figure 17 is the same figure as Figure 16, but over the tropical eastern Pacific Ocean. In Figures 17 (a) and (b), it can be recognized that the precipitation difference between CTRL and CMAP is excessively larger than that between TEST and CMAP around the ITCZ. Over the region, the precipitation rate departure of CTRL from CMAP is excessively larger than that of TEST3 over the ITCZ precipitation band found in Figure 17 (c). This region corresponds to where the excessive strengthening of the precipitation inside the ITCZ can be recognized in Figure 15 (a). Table 4 (b) is the same table as Table 4 (a), but over the tropical eastern Pacific Ocean (30S - 30N and 120W -

60W). The RMSE and MD become a little worse by assimilating the AMVs. These results show that the AMV data seems to have a neutral or negative impact on the precipitation field over the tropical eastern Pacific Ocean.

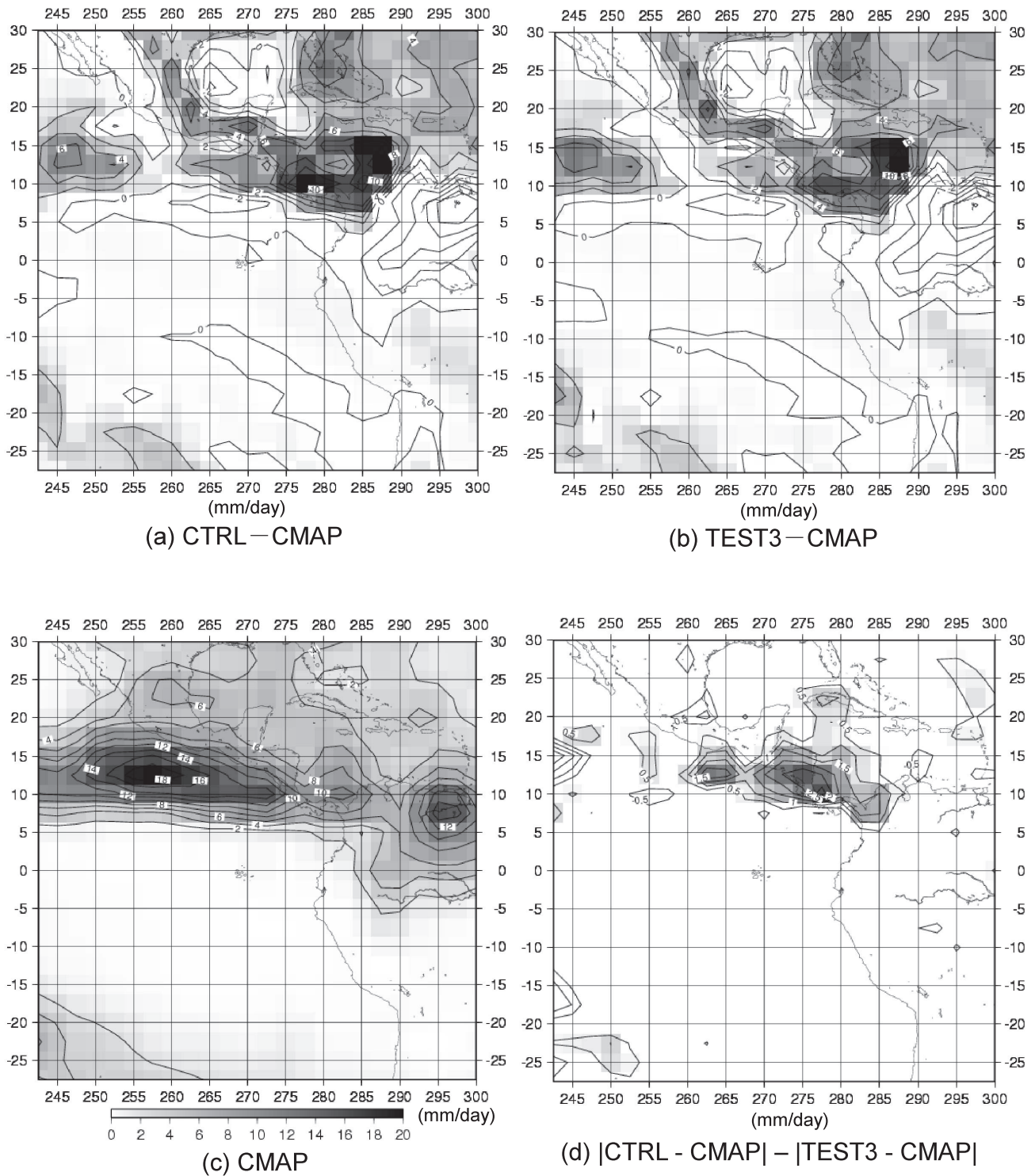


Figure 17: Same figure as Figure 16, but over the tropical eastern Pacific Ocean (30S-30N and 120W-60W).

5. Summary

In this investigation, the characteristics and impacts used in JRA-25 were examined. Firstly, the AMVs used over the entire JRA-25 period were reviewed. Over the entire period of JRA-25, the slow wind biases of the AMVs toward the background wind fields were recognized in the GMS, METEOSAT and GOES AMVs. These slow biases were mainly observed in the upper tropospheric AMVs over the northern and southern hemisphere extra-tropics, and were larger in the winter hemisphere. It was found that generally the biases decrease year by year. In comparison to past investigations by Källberg and Uppala (1998) on ERA-15 from 1979 to 1993, the interannual variation in AMV quality recognized in JRA-25 is similar to that in ERA-15. In particular, after 1996 the biases in the GOES AMVs were smaller than the other AMVs because of the introduction of wind and height adjustments.

Reviewing the AMV data for July 2003 which is used in the OSE to investigate the impacts of the AMVs, the upper tropospheric IR and WV winds of the MSC AMVs which were computed from images observed by the GOES-9 located at 155E and the METEOSAT AMV, contain significantly slow biases over the northern and southern hemispheres. The slow biases are larger in the southern hemisphere where it is winter in July. Moreover, the biases in the IR winds are larger than those in the WV winds. Källberg and Uppala (1998) also indicate that AMV data has a tendency to reduce the west-east component of the analysis wind between 150 and 200 hPa in both hemispheres. Both the results gained in JRA-25 and ERA-15 closely correspond to each other.

Biases were observed in both easterly and westerly winds, and were larger in higher

speed ranges, except for easterly winds in the METEOSAT-5 IR-wind over the southern hemisphere. Regarding GOES-10 AMVs, the slow biases were small because of the wind speed and height adjustments implemented in GOES-10 AMV retrieval. The Departures in the west-east component of the lower tropospheric AMVs were small. Over the tropics and the southern hemisphere, the Departures had slightly positive values.

To review the impact of the AMV data on JRA-25, the OSE was examined for the case of July 2003. Over the tropical Indian Ocean, the upper and middle tropospheric easterly winds were strengthened over the Equator by assimilating the AMV data. In addition, the upper tropospheric anticlockwise wind circulation arising from the Indian monsoon was strengthened. It was also recognized that the upper tropospheric AMVs contribute to the modification of precipitation over the region more effectively than the lower tropospheric AMVs. Evaluation of the precipitation fields by CMAP shows that the AMV impacts over the tropical Indian Ocean are almost neutral, but small shifts in precipitation were recognized.

Over the tropical eastern Pacific Ocean, lower tropospheric convergence to the south of the ITCZ was strengthened by assimilating the upper and/or lower tropospheric AMVs. Convergence strengthening caused the intensification of ITCZ precipitation. Evaluating the precipitation by CMAP shows that the AMV impact seen over the region is slightly negative. One possible reason to explain this result except for the period of selection is that this region is located in the large satellite zenith angle region of the GOES-10 and GOES-12 observation range. Generally, it is difficult to

produce AMVs in such regions because of the lower spatial resolution of satellite image data and the difficulty of estimating radiation absorption by the atmosphere. It is possible that this factor distorted the JRA-25 wind field in this region. However, further investigations are needed in order to obtain a valid interpretation.

Acknowledgement

The author is grateful to M. Tokuno of the MSC/JMA for the support and advice in submitting this paper. The author's appreciation also extends to the JRA-25 project members at the JMA, M. Sakamoto, S. Kobayashi, T. Matsumoto, H. Koide, K. Onogi and T. Ose for their technical support and advice, together with the utilization of computing devices for this investigation. Thanks also go to T. Imai, D. Uesawa, Y. Tahara and T. Kurino of the MSC/JMA, N. Ohkawara of the CPD/JMA, and H. Yamashita and Y. Sato of the NPD/JMA, for their valuable support and advice.

References

- Daniels, J., Bresky, W., C. Velden and S. Wanzon, 1998: Recent advances to the operational GOES wind processing system at NESDIS, Proc. of '4th International winds workshop', EUMETSAT, 29-39.
- Fiorino, M. 2002: Analysis and forecasts of tropical cyclones in the ECMWF 40-year reanalysis (ERA-40). Extended abstract of 25th Conference on Hurricanes and Tropical Meteorology, 261-264.
- Gruber, A., X. Su, M. Kanamitsu, and J. Schemm, 2000: The comparison of two merged rain gauge-satellite precipitation datasets. Bull. Amer. Meteor. Soc., 81-11, 2631-2644.
- Holmlund, K., 1998: The utilization of statistical properties of satellite-derived atmospheric motion vectors to derive quality indicators, Weather and Forecasting, 13, 1093-1104.
- Hayden, C. M., 1993: Recent research in the automated quality control of cloud motion vectors at CIMSS/NESDIS, Proc. of 'Second International Winds Workshop', EUMETSAT, 219-226.
- Ishii, M., A. Shouji, S. Sugimoto and T. Matsumoto, 2005: Objective Analyses of Sea-Surface Temperature and Marine Meteorological Variables for the 20th Century Using ICOADS and the KOBE Collection. Int. J. of Climatology, 25, 865-879.
- Källberg, P. and S. Uppala, 1998: Impact of Cloud Motion Winds in the ECMWF ERA15 Reanalysis. Proc. of 'Fourth International Winds Workshop', EUMETSAT, 109-116.
- Kumabe, R., 2004: Renewal of operational AMV extraction system in JMA. Proc. of 'Seventh International Winds Workshop', EUMETSAT, 71-77.
- Nakamura, Y., 2004: The project of Global Spectral Model development (Part 1). Additional volume No.50 of Numerical Prediction Department Report, Forecast Division of Japan Meteorological Agency, 110-115 (in Japanese).
- Nieman, S., J. Daniels, D. Gray, S. Wanzong, C. S. Velden and W. P. Menzen, 1996: Recent performance and upgrades to the GOES-8/9 operational cloud-motion vectors. Proc. of 'Third International Winds Workshop', EUMETSAT,

31-36.

Ohkawara, N., T. Imai and R. Kumabe, 2004: Development the High-density Atmospheric Motion Vector Product. Meteorological satellite center technical note, 45, 1-16 (in Japanese).

Onogi, K., H. Koide, M. Sakamoto, S. Kobayashi, J. Tsutsui, H. Hatsushika, T. Matsumoto, N. Yamazaki, H. Kamahori, K. Takahashi, K. Kato, R. Oyama, T. Ose, S. Kadokura and K. Wada, 2005: Japanese 25-year Reanalysis --- progress and status ---, QJRMS special issue on the WMO 4th Data Assimilation Conference, Q. J. R. Meteorol. Soc., 131, 3259-3268.

Rattenborg, M., 1998: Status and development of operational METEOSAT wind products, Proc. of 'Fourth International Winds Workshop', EUMETSAT, 49-59.

Walter, R. J., 1993: Current status of the operational wind extraction program in NOAA/NESDIS. Proc. of 'Second International Winds Workshop', EUMETSAT, 43.

Van de Berg, L., J. Gustafsson and A. Yildirim, 2002: Reprocessing of atmospheric motion vectors from METEOSAT image data. Proc. of 'ERA-40 workshop on Re-analysis', 5-9.

WMO, 1988. World Meteorological Organization Manual on Codes, Publication 306, Volume 1, Part B, Supplement No. 3. Contains the official descriptions of the code form for BUFR and GRIB.

JRA-25 長期再解析で使用された大気移動風 (AMV) の特徴と有効性に関する調査

小山 亮

要 旨

JRA-25 長期再解析は、気象庁 (JMA) と電力中央研究所 (CRIEPI) による、1979 年から 2004 年に渡って世界的かつ均質なデータを作成するプロジェクトである。この解析値データを利用することにより、過去の気候の推移の正確な把握、気候モデルの高度化とともに、3 次元かつ空間的に均質なアプローチによる全球的な気候および気象事例の調査が可能である。

JRA-25 に使用された大気追跡風 (AMV) データの品質と特性、及び風や他の物理量の解析場を与える効果について調査を行った。その結果、全期間の MSC (Meteorological Satellite Center) AMV、METEOSAT (Meteorology Satellite) AMV、及び 1995 年以前の GOES (Geostationary Operational Environmental Satellite) AMV に対流圏上層で風速のスローバイアスが見られ、特に冬半球で顕著であった。このスローバイアスは年々減る傾向にあった。これらの特徴は ERA-15 (ECMWF 15 year reanalysis) でみられた AMV の特徴とよく一致していた。

AMV が解析場を与えているインパクトを調べるために、2003 年 7 月の期間で観測システム実験を行った。AMV の同化によって、インド洋熱帯域では、上層の東風及び反時計回りの循環が修正され、対流圏上層及び下層の水平発散場が修正された。東太平洋熱帯域では、対流圏上層及び下層の風場が修正され、熱帯収束帯 (ITCZ) 付近の下層の収束場を強化していた。これら 2 つの領域で下層の水平発散場のインパクトに対応した降水の分布の変化が見られた。この降水へのインパクトは、CMAP (Climate Prediction Center (CPC) Merged Analysis Precipitation) 降水量データとの比較では、インド洋域では中立、東太平洋域では ITCZ の近傍でややバイアスが大きくなる傾向がみられた。